University of Stavanger

FACULTY OF SCIENCE AND TECHNOLOGY

MASTER'S THESIS

Study programme/specialisation: Petroleum Engineering, Drilling and Well Engineering	Spring semester, 2021 Open / Confidential
Author: Fiona Øijordsbakken Fredheim	
Programme coordinator: Hans Joakim Skadsem Supervisor(s): Hans Joakim Skadsem	
Title of master's thesis: An Experimental Study of Vibration Assisted Displacement in a Horizontal Annulus for enabling Through Tubing Abandonment	
Credits: 30	
Keywords: Through- Tubing Abandonment Displacement Efficiency Vibration tool Permanent Plug and Abandonment Light Well Intervention Vessel	Number of pages: …76…… +supplemental material/other: …7…… Stavanger, 11.07.2021…….. date/year

Abstract

Traditionally, Permanent Plug and Abandonment (PP&A) operations has been carried out by pulling casing and tubing using either Mobil Offshore Drilling Unit (MODU) or Fixed Platform Drilling (FPD). The costs can run up to 25% of the total well, therefore, new cost-efficient PP&A technology is a necessity (Khalifeh & Saasen, 2020b). In later years Through-Tubing Abandonment (TTA) has been viewed as a good alternative, by not having to pull any casing or tubing and thus saving rig time. This method can also be used on a Light Well Intervention Vessel (LWIV) to further reduce the costs significantly (Thom, Angell, Greig, Robertson, & Hogg, 2020). However, a challenge with this method that causes great concern, is whether the drilling fluid will be properly displaced and removed in the annulus due to lack of tubing centralization and possibly unfavorable flow dynamics.

To study how the TTA method can be improved, this thesis aim to investigate the effect of vibration at different frequencies and eccentricities in laboratory experiments using a vibration tool, with a particular focus on enabling TTA. The experiments was carried out using a test rig built at Norwegian Research Centre (NORCE). The test rig is a downscaled annulus made out of a steel tubing and a transparent casing and fitted with a vibration motor for moving the inner tubing. In these experiments, flow rate, densities and viscosities of the displacing and displacement fluids were designed by the use of dimensional analysis to reflect a real-life operation. These parameters were kept constant while eccentricity and vibration was varied to investigate their effect on the displacement process. The allocated laboratory time period was unfortunatly shortened due to time constraint caused by the COVID-19 pandemic. A total of 26 test runs was carried out, where 12 test runs was used in this study.

The findings in these experiments indicates that gravity is the dominating force for this system, consequently resulting in an undesired slumping displacement front. Nevertheless, as eccentricity increases, the gravitational force becomes less dominant and a more even and steady piston like displacement front is observed. Moreover, the results indicates that high vibration will promote fluid to flow in the entire area of the annulus; both on the upper wide part and the lower narrow part. This results in a more evenly distributed and steadier displacement front. But in this study, the low- and medium- vibrations does not appear to significantly improve the displacement efficiency. In spite of this, it is noteworthy to mention that vibration has been found to be a useful tool for decreasing undesirable high yield- and gel strengths in old drilling fluid (Thom et al., 2020).

Acknowledgement

Firstly, I would like to express my sincere appreciation to my supervisor Associate Professor Hans Joakim Skadsem who has motivated and guided me throughout this semester with his vast knowledge in the subject of matter. I would also like to express my sincere thanks to Researcher at NORCE Jonas Kristoffer Sunde for all the help provided at NORCE.

Finally, I wish to express my great gratitude to Specialist Well Technologies Surface Wellhead & Tress System at Equinor, Dag Ketil Fredheim, for valuable discussions and provide insightful comments.

Table of Content

Nomenclature

Abbreviations

CDF	Computational Fluid Dynamics
ELF	Effective Laminar Flow
FPD	Fixed Platform Drilling
LWIV	Light Well Intervention Vessel
MODU	Mobile Offshore Drilling Unit
P&A	Plug and Abandonment
PP&A	Permanent Plug and Abandonment
TTA	Through- Tubing Abandonment
VFD	Variable Frequency Driver
At	Atwood number
Fr	Froude number
Re	Reynolds number
OD	Outer diameter
ID	Inner diameter

List of Symbols

$\hat{\rho}$	Density
$\hat{t}$	Time
$\vec{\hat{v}}$	Velocity
$\hat{\mu}$	Viscosity
$\vec{\hat{g}}$	Acceleration of gravity
D_H	Hydraulic diameter

L	Length
M	Mass
V	Volume

List of Figures

List of Tables

1 Introduction

When a well reaches the end of its lifetime and the production of oil and/or gas is no longer viable, the well must be Permanently Plugged and Abandoned (PP&A). Traditionally, PP&A operations has been carried out by cutting and pulling casing tubing using Mobil Offshore Drilling Unit (MODU) or Fixed Platform Drilling (FPD). The oil companies' cost of PP&A of wells has become continuously more important as requirements and regulations as well as complexity has increased and may be as high as 25 % of the total costs (Khalifeh & Saasen, 2020b).

Recently the Through-Tubing Abandonment (TTA) method has shown to be a very cost-effective alternative. TTA means to abandon the well without pulling the tubing; the cement is pumped down the tubing and into the annulus through perforations just above the mechanical plug. This will create a solid cement plug both in annulus and in tubing and will be a part of the secondary barrier system. The advantages of using TTA is saving costs by not having to pull any casing or tubing and therefore saving rig time. This method can also be used on a Light Well Intervention Vessel (LWIV) to further reduce the costs significantly (Thom et al., 2020).

However, there is a significant challenge that needs to be addressed first; the removal and displacing of drilling fluid in the annulus. The drilling fluid displacement can become especially difficult where the annulus is no longer centralized. A non-centralized annulus with a narrow side can prevent displacement flow, and thus the cement quality deteriorates.

It is well acknowledged that casing rotation/reciprocation (particularly rotation) helps mobilize the drilling fluid that would otherwise be trapped on the narrow side of the annulus. This increases the displacement efficiency and facilitates for a more steady displacement. Unfortunately, rotation and reciprocation are not possible for TTA, but the industry has investigated the feasibility to utilize other tools such as a downhole vibration tool.

This thesis aims to investigate the effect of vibration at different frequencies and eccentricities in laboratory experiments using a vibration tool.

1.1 Objectives

The main purpose of this thesis is to study the effects of tubing vibration in displacement efficiency in an eccentric horizontal annulus. The objectives for the investigation are listed below:

- Study how varying the vibration intensity affect annular displacement.
- Study how varying degrees of eccentricity affect annular displacement.
- If there under any conditions exists a steadier displacement pattern.

1.2 Limitations

This thesis is limited to the investigation of TTA displacement for non-hardening Newtonian fluids with low density contrasts and low viscosities with a relatively short test section and low flow velocity. The flow regime studied are laminar for both the displaced- and the displacing fluid. Displacement involving non-Newtonian fluids, high flow velocity, turbulent flow regimes, high viscosity, immiscible fluids (e.g. oil with water) and hardening fluids will not be considered in this thesis.

1.3 Structure of Thesis

Chapter 1 provide an overview of the thesis, the objectives and limitations. The theory is introduced in Chapter 2 where the theoretical result is presented. This includes an overview of barriers and cementing operation, displacement in cementing, the effect of casing movement, fluid design, dimensional analysis of the experiment and previous research. Chapter 3 is a description of the methodology of the experiments, including dimensions and apparatus. The data is then applied along with the theoretical results for further understanding of the fluid mechanics of the displacement process in the presence of tubing vibration. The results are presented and discussed in Chapter 4. Lastly, the main observations and results are summarized in Chapter 5, as well as recommendations of further work.

2 Theory

2.1 Overview of Barriers and Cementing

This thesis will examine the application of vibration in horizontal wells to assist cement displacement and thereby improved cement barriers. Therefore, a general overview of barriers and the well cementing operation is presented in the following sections.

2.1.1 Barriers

The prime objective of permanent well abandonment is establishing permanent barriers, preventing hazardous fluids from flowing uncontrolled into the surroundings. “application of technical, operational and organizational solutions to reduce risk of uncontrolled release of formation fluids throughout the life cycle of a well” ("NORSOK Standard D-010," 2021). The Norwegian regulatory organ imposes that the failure of a single barrier shall not lead to unfortunate consequences. Therefore, a verified rock-to -rock barrier envelope is vitally important. The required internal cement plug length of good cement, with a qualified annular cement barrier is 30 meters ("NORSOK Standard D-010," 2021) . Figure 2.1 gives a schematic example of a TTA cement plug.

However, in TTA wells, placing qualified barriers may be challenging due to eccentricity, presence of control lines, minimal clearance between the pipe and the casing and drilling fluid contamination. If drilling fluid is contaminating the cement slurry or creates channels, the cement may lose its integral strength and may not act as a proper barrier element (Khalifeh & Saasen, 2020b).

This thesis will examine this problem and study if applying vibration in a horizontal well will improve displacement, and thereby, the quality of the cement as a barrier.

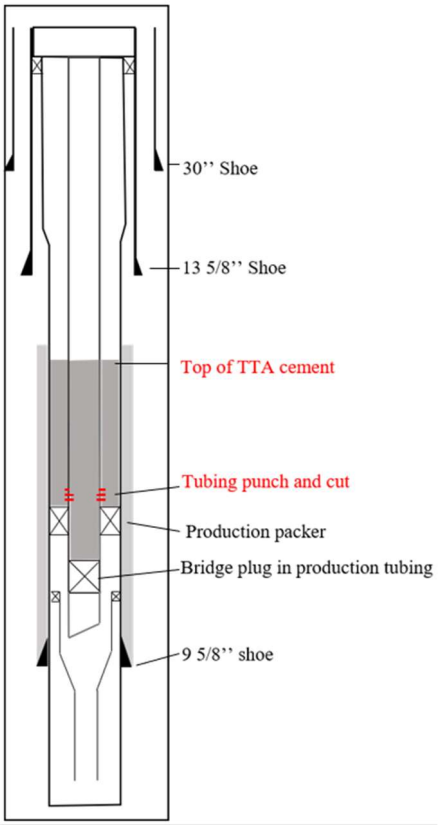

Figure 2.1 – TTA barrier plug schematic. This is an original Figure that is based on the figure from Thom, F. et. Al (2020).

2.1.2 Well cementing

The cementing job is a crucial well operation, the key objective is to obtain zonal isolation in the wellbore and prevent leakage. In terms of P&A operations, this means to create a cross-sectional barrier, also known as a rock- to- rock barrier. To achieve this objective, a hydraulic seal is created between the formation and casing and in the wellbore to prevent fluid channels in the cement. During the establishment of the well, the cementing process is known as primary cementing. The purpose of this operation is to remove drilling fluid and additional residuals from the well, replacing it with a suitable cement slurry. In this process, a sequence of fluids is pumped down through the casing to bottom of the well, where it returns to surface through the annulus. This sequence process is often called the cementing displacement. The displacement describe the ability of one fluid to displace another from the annulus. The

process is completed when a pressure increase at surface is detected, this indicates that the top of cement has reached the landing collar and the displacement of drilling fluid is complete. Finally, the cement slurry is left to settle and harden before drilling continues.(Nelson & Guillot, 2006) This cementing process is highly similar to though tubing abandonment cementing. Therefore, primary cementing theory can be applied to TTA cementing.

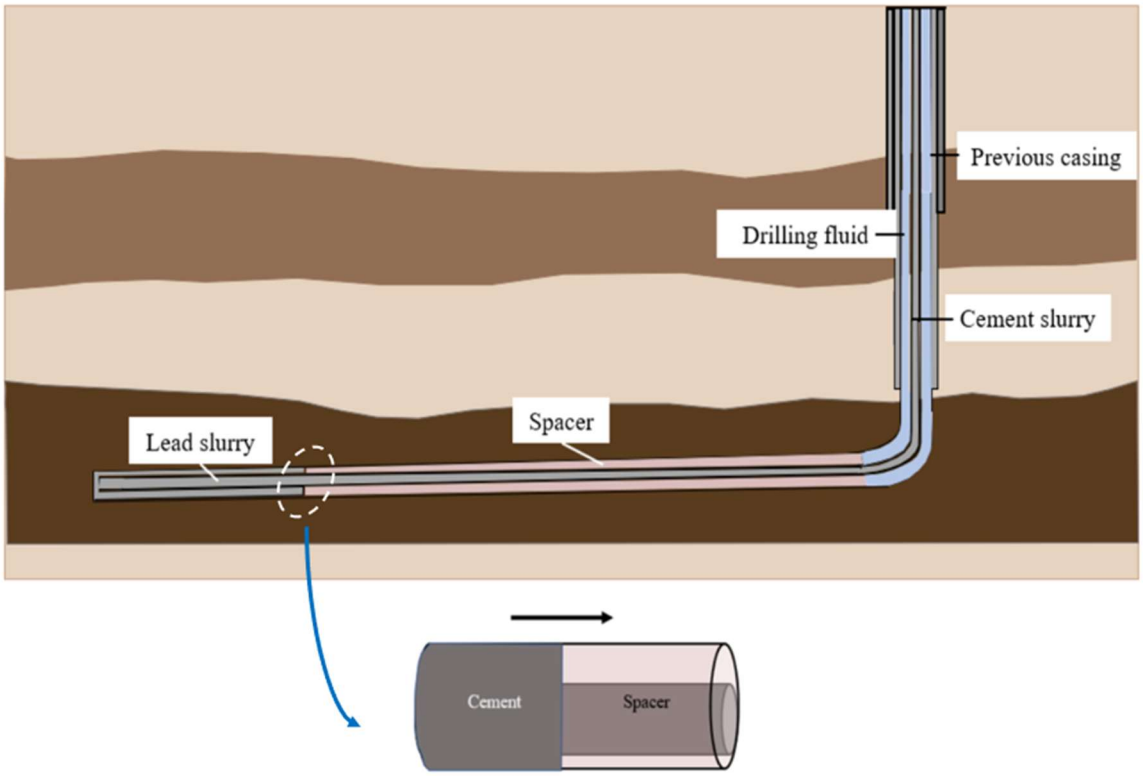

Figure 2.2 – Schematic of horizontal cementing, where cement displaces the spacer fluid

2.1.3 Cementing practices for horizontal cementing

New technology made it possible to align the well horizontally with the reservoir. Therefore, an upsurge of horizontal drilling, and thus, horizontal cementing has been seen the last 30 years. Although the method of drilling and cementing horizontally has become the prevailing method, high numbers of cement leakage is documented for such wells. These high numbers may be associated with the additional challenges specific to horizontal and deviated wells. Keller et. al. (1987) presented a paper concerning the difficulties of cementing deviated wells. Some of the major issues concerns solids settling from the fluid to the bottom side of the

annulus. This may create continuous drilling fluid channels on the bottom side of the annulus which can adversely affect the displacement efficiency (Keller, Crook, Haut, & Kulakofaky, 1987). This will be furthered discussed in Chapter 2 Section 2.1 Displacement in The Annulus.

2.2 Displacement in the Annulus

In a well cementing operation, displacement efficiency is used to describe the ability of one fluid to displace another from the annulus. The well flow is a sequence of fluids where each fluid displaces the one in front. During a cementing operation, the sequence of the fluids would respectively be drilling fluid followed by a spacer fluid followed by a cement slurry. The objective of this sequence is to fully remove the drilling fluid, prepare the well for cement placement and completely fill the desired area of the annulus with cement slurry.

The displacement efficiency at time t > 0 is equal to the volume fraction of displacing fluid in the system. The rate of displacement is often referred to as displacement efficiency, it can be defined as follows:

$$Displacement\ Efficiency = \frac{Volume\ of\ Dispacing\ Fluid\ in\ Annulus}{Annular\ Volume}$$

In an ideal displacement, the displacing fluid perfectly displaces the displaced fluid. This means that the shape of the interface of the fluids advances steadily long the displacement area at the same fluid velocity. And hence, the interface shape must be constant along the displacement area. Such an ideal displacement is often called a steady displacement (Renteria 2020). Figure 2.2.1 gives a typical example of such a process.

The quality of the displacement has significant impact on the cement quality and the zonal isolation and it therefore a subject of great interest (Nelson & Guillot, 2006). The factors influencing the displacement process such as, flow regimes, friction, eccentricity, inclination and hole conditioning will be discussed.

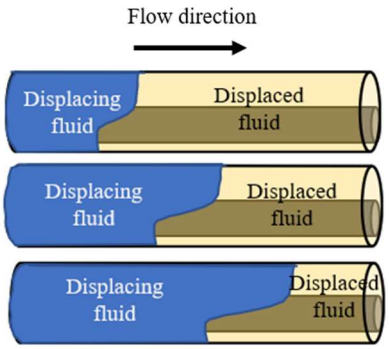

Figure 2.2.1 – Illustration of a typical displacement process of a denser more viscous cement slurry displacing a lighter less viscous spacer fluid .

2.2.1 Flow Regimes

The flow regimes of an annular hole are classified as either laminar, turbulent or transient. Generally, a flow is defined as laminar if the Reynolds Number (Re) is less than 2300 and turbulent if Reynolds number e is greater than 4000. The transition zone exists between 2300 and 4000. The laminar flow is characterized by smooth streamlines, whereas turbulent flow is rather chaotic with fluctuations in the streamline (Çengel, Cimbala, & Turner, 2017).

Normally, cement slurries have a high viscosity and density. These properties suppress fluid fluctuations resulting in a laminar straight flow. In turbulent flow, the internal forces are greater than the viscous forces, hence, high degree fluctuations dominate the flow (Çengel et al., 2017). Flow velocity significantly affect the fluid regime, especially for drilling fluids and spacer fluid . At low velocities, both drilling fluids and spacer fluids are characterized as laminar, while they are turbulent at high velocities. In Figure 2.2.2, both laminar and turbulent flow regimes are illustrated. As shown, the average annular velocity profile (red line) and the actual annular velocity profile (black) are not equal. Furthermore, the axial velocity (arrows) in the turbulent flow is more uniform throughout the annulus, than in the laminar flow regime. Thus, turbulent flow regimes will generate higher velocities at the boundaries of the pipe than laminar flow regimes. Due to friction at the pipe walls, the maximal axial velocity is in the center of the pipe and is decreasing at the boundaries. Therefore, it is more challenging to remove drilling fluid at the pipe walls. This problem can further be connected to contamination of the cement; when drilling fluid is left behind in the wellbore, drilling fluid channels are formed in the cement slurry. These drilling fluid channels have disadvantageous properties and will adversely affect the cement quality (Khalifeh & Saasen, 2020a). It was

shown by Haunt & Hook (1979) that cement contamination is caused by instabilities in the drilling fluid-cement interface where the axial velocities are not truly axial (vertical). The interface instabilities are a consequence of nonlinear coupling of changes in share stress and shear rate (Haut & Crook, 1979).

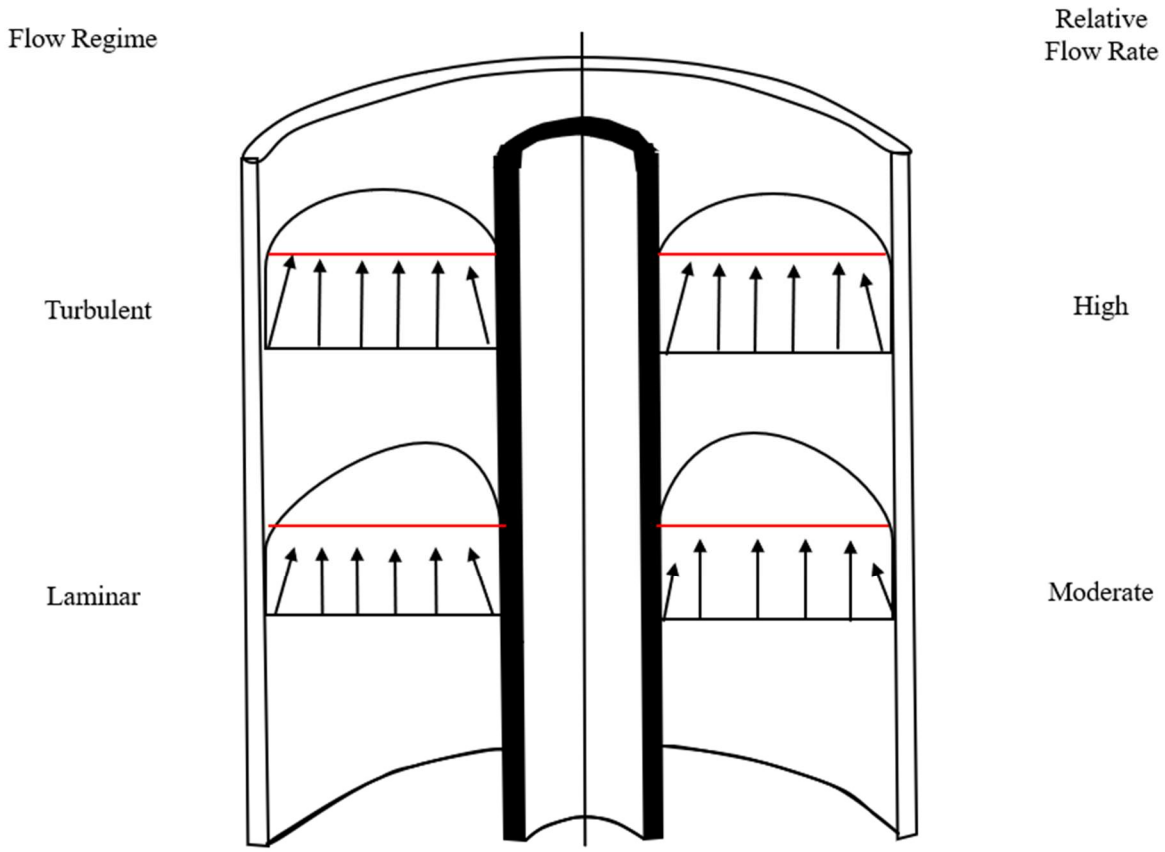

Figure 2.2.2 – Flow regimes in an annulus. This is an original Figure that is based on the figure from Khalifeh & Saasen (2020).

2.2.2 Wellbore Eccentricity

During a cementing operation the pipe is usually not perfectly centered in the wellbore. This deviation is referred to as eccentricity and is used to describe how off-centered a pipe within another pipe is. The degree of eccentricity can be described as follows:

$$Eccentricity = \frac{w_{min}}{R_{casing} - R_{tubing}} * 100\%$$

W_{min} denotes the minimum distance between the casing and tubing, R_{casing} and R_{tubing} are respectively the radii of casing and tubing. For instance, a pipe would be considered fully eccentric if the pipe is in contact with either side of the enclosing casing (100% eccentric). If the pipe is perfectly centralized in the well it is concentric (0 % eccentric) (Lavrov & Torsæter, 2016a).Figure 2.2.3 shows examples of different eccentricity percentages of a tubing within a casing with its corresponding displacement profile.

Eccentricity is one of the key difficulties in carrying out an efficient displacement process. Eccentricity stimulates fluids to move faster where the gap is at its widest, to the path of least resistance. By contrast, fluid flow on the narrow side is obstructed by the eccentricity. For instance, in a displacement process where cement displaces a spacer fluid , eccentricity can hinder uniform fluid flow. The spacer fluid in the narrow side of the annulus will then be bypassed, leading to poor displacement efficiency as shown in Figure 2.2.4.

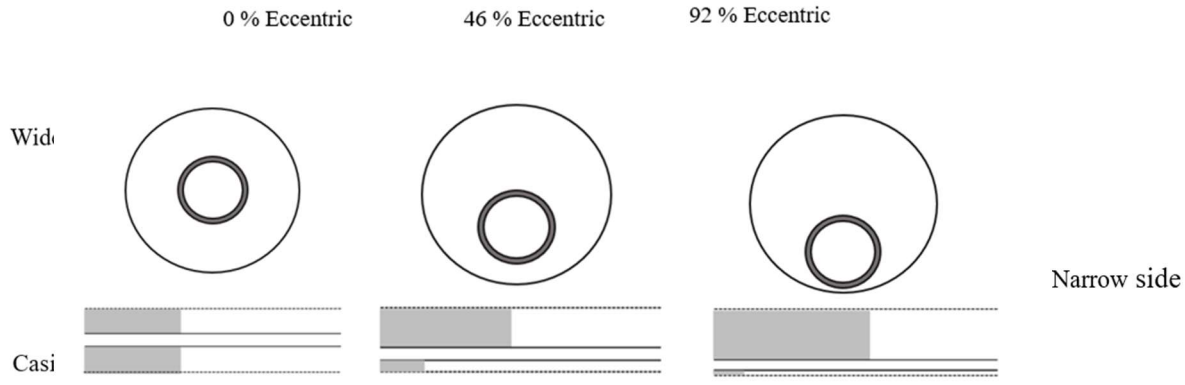

Figure 2.2.3 – Illustrates eccentric annuli, with respectively 0 %, 46 % and 92 % eccentricity with their corresponding displacement profile.

2.2.3 Inclination

Inclined and horizontal wells are subjected to additional factors which complicate the displacement process, such as gravity-induced eccentricity and particle sedimentation. Eccentricity is common in both vertical and inclined wells, however, in an inclined well, the eccentricity may be intensified by gravity, thus complicating the displacement process. Figure 2.2.5 illustrates an example of particle sedimentation where gravity acts on the solid particles (weighing agents such as barite) in the drilling fluid. This causes the particles to settle, and thus thickening the drilling fluid on the narrow part of the annulus. Displacement of thicker drilling fluid may require higher flow rates and higher rheological properties that make the displacement process more difficult (Lavrov & Torsæter, 2016a).

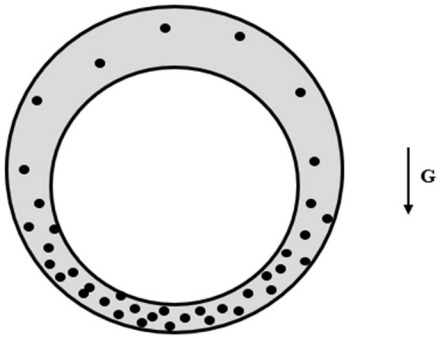

Figure 2.2.5 – Solids settling and accumulating in inclined/ horizontal

2.2.4 Gravity (Buoyancy) vs. Eccentricity

In a horizontal annular displacement, there is a counteraction for the displacement front between gravity (buoyancy) and eccentricity. Eccentricity promotes the fluid flow to the wider part of the annulus while the gravity promotes stable stratification (the front layer is less dense than the one behind it). This results in either a ‘top side’ or ‘slumping’ displacement front, see Figure 2.2.6 In the ‘top side’ displacement, the effect of eccentricity is dominant. The displacement front will then elongate along the upper wider part of the annulus. In slumping displacement, the effect of gravity dominates, and the displacement front will be driven to the narrow lower side of the annulus and elongate. Both the ‘top side’ and slumping

displacement front results in an unstable displacement. Ideally the displacement front should be stable and propagate steadily at the same pumping speed both on the upper and lower part, Figure 2.2.6) display an ideal displacement where the effect of eccentricity and gravity equalizes each other. In a horizontal annulus however, this displacement front is very difficult to obtain.

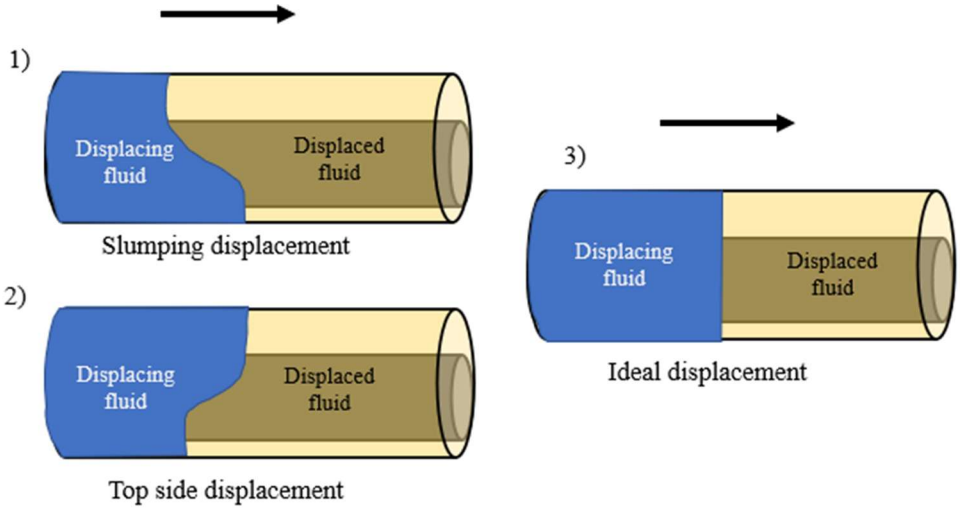

Figure 2.2.6 – Different types of displacement fronts. 1) Slumping displacement, 2) Top side displacement and 3) Ideal displacement

2.2.5 Hole Conditioning

Drilling fluids are designed to have a relatively high viscosity and gel strength to contribute to good cuttings transport and efficient drilling operations. However, these properties are not suitable for good and effective drilling fluid displacement. Thus, before conducting a cementing operation, the well must be modified to a suitable condition. There are essentially two properties that need to be reduced: rheology and density. Although, it is also generally necessary to also reduce gel strengths, plastic viscosity, and yield strengths. By reducing these parameters, the restricting forces of drilling fluid flow are reduced and consequently enables a more efficient drilling fluid displacement (Khalifeh & Saasen, 2020a).

2.3 Effect of Pipe Movement

It is well recognized that pipe movement benefits the displacement efficiency. From primary cementing, pipe rotation is considered as part of "good cementing practices" (Nelson & Guillot, 2006). The enhancement is due to drag force being applied from the pipe to the drilling fluid which induces shear stress and therefore fluid movement. This is particularly advantageous in an eccentric annulus where flow on the narrow side is assisted as a result of the fluid movement (Lavrov & Torsæter, 2016a).

The TTA is primarily relevant for LWIV (light well intervention vessel) operations where conventional rigs are either not possible or too expensive to execute. For LWIV operations, casing rotation and is not an alternative. Therefore, a vibration tool will act as the pipe movement for operations involving LWIV. However, even though vibration is considered in this thesis, it is useful to consider rotation and reciprocation due to the similar effects both the rotation and vibration have on displacement efficiency.

2.3.1 Vibration in the Well

Downhole vibrations are primarily classified as either axial, lateral or torsional. These three vibration classifications generate different vibration patterns as seen in Figure 2.3.1 Axial vibration generates movement in the vertical direction of the well. The axial vibration is damped as the vibration travels to the surface through the casings, and thus, is considered as the least aggressive vibration mode. Lateral vibration is the side – to – side motion in the horizontal direction, which creates a whirling wave in the wellbore. Torsional vibration generates twisting motion in the casing/tubing and is most similar to rotational motion of the three vibration modes (Aadnøy & Society of Petroleum, 2009).

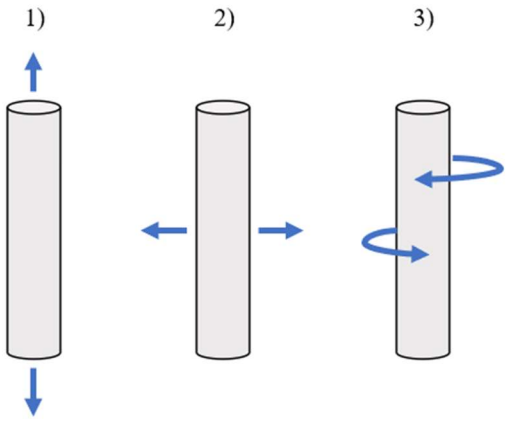

Figure 2.3.1 – Vibration in the well. 1) axial vibration 2) lateral vibration 3) torsional vibration

2.3.2 Casing Rotation and Reciprocation

In a primary cementing operation, there are two methods of pipe movement: rotation and reciprocation. Reciprocation is the movement where the pipe is alternately raised and lowered in the wellbore. It is usually limited to 9 m to 18 m of vertical travel in addition to axial movement (Schlumberger, 2021). However, there are some disadvantageous features of reciprocation, such as surging and swabbing of the bottomhole pressure: this can result in stuck pipe, formation fluid influxes, wellbore instabilities and fluid losses. Pipe rotation does not contribute to any of these disadvantages and is thus favored (Lavrov & Torsæter, 2016a).

Casing rotation becomes increasingly important when the well is subjected to non-ideal conditions, such as eccentricity. When the pipe is rotated at high speed, it starts to have an orbital movement inside the casing, in addition to rotation around its own axis. An orbitational flow called Taylor vortices is then generated. The Taylor vortices creates helicoidal or toroidal flow patterns as shown in Figure 2.3.2 These Taylor vortices are particularly helpful in facilitating flow in the narrow part of the annulus and prevent particle sedimentation.(Nelson & Guillot, 2006).

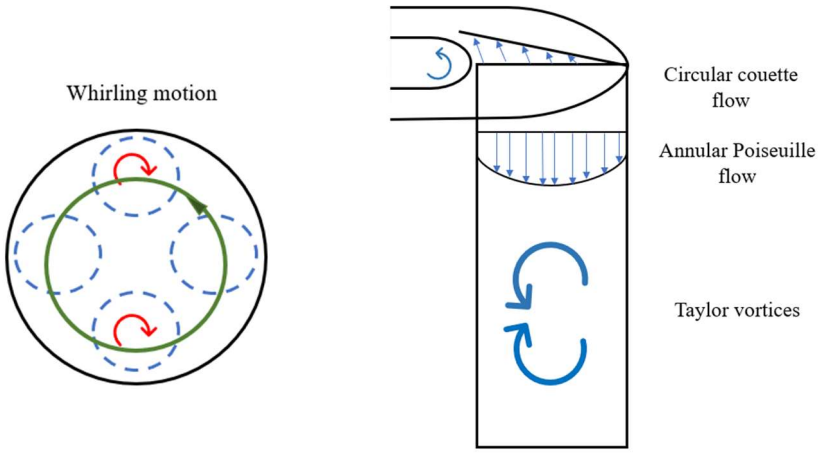

Figure 2.3.2 – Show the whirling motion created by rotation and how Taylor vortices will flow in the annulus. This is an original Figure that is based on the figure from Nelson, E. B., & Guillot, D. (2006).

Although it is quite difficult to exactly measure the effect of rotation, experiments and simulation can, to a certain extent, provide good insight (into the impact of pipe rotation). Enayatpour and van Oort (2017) investigated by CFD simulation, the effect of several parameters impacting displacement efficiency, including pipe movement. They found that pipe movement, especially rotation, increased displacement efficiency and counteracted the negative effect of eccentricity. Figure 3.3.3 illustrate the effect of rotation on displacement efficiency for two fluids. We see that the pipe being subjected to 20 RPM (blue line) has a smaller fraction of non-displaced fluid (e.g. spacer fluid) compared to the pipe not subjected to any rotation (red line). Thus, pipe rotation appears to improve displacement efficiency.

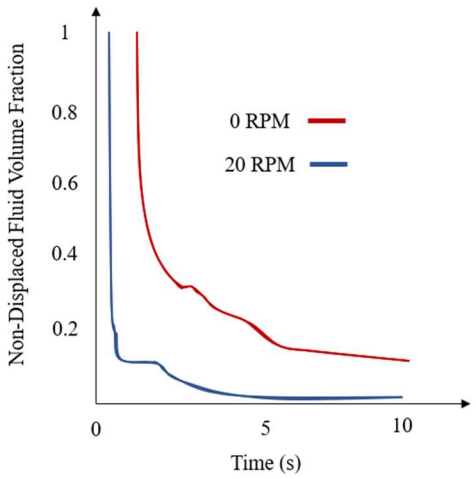

Figure 2.3.3 – Effect of rotation on displacement efficiency for two fluids. Blue graph displays the effect of the pipe being subjected to 20 RPM, while Red is kept still. The graph shows the change of non-displaced fluid fraction as a function of time.

2.4 Fluid Design

The sequence of fluids in a cementing operation consists of drilling fluid followed by a spacer fluid and finally followed by a cement slurry. The fluid volumes are pumped in such an order that we can consider each displacement process as consisting of two fluids only. In this study, the displacement sequence of a Newtonian spacer fluid followed by a Newtonian cement slurry is considered.

2.4.1 Drilling Fluid

The drilling fluid is either oil-or water-based. Its main functions are removal of cuttings, solids suspension avoiding solids settling, prevention of uncontrolled reservoir fluid inflow to the well, forming a filter cake on the wellbore walls to seal pores, and maintaining a chemical reactivity stabile wellbore. Drilling fluids are non-Newtonian and often with a yield stress (Caenn, Darley, & Gray, 2016). Having a yield stress, τ_y (Pa) means the liquid requires an excess of shear stress up to a certain threshold value to be enable it into motion (Lavrov & Torsæter, 2016b).

2.4.2 Spacer Fluid

Spacer fluids (or washers) is an umbrella term for any fluid which physically separates a liquid from another. In a cementing operation, the spacer fluid is designed to separate the drilling fluid from the cement slurry. This is to provide a buffer between them and minimizing mixing. The spacer fluid is intended to displace (remove) the drilling fluid and ensure water-wetting of the surfaces to ease the cement bonding to either the formation or the casing. The spacer fluid should be compatible with the drilling fluid and should not affect any of the properties of the cement slurry such as viscosity or yield strength. The spacer fluid being displaced by cement is typically Newtonian with low density and viscosity (Khalifeh & Saasen, 2020a).

2.4.3 Cement Slurry

The principal function for a cement is to prevent uncontrolled fluid movement in the well by establishing a seal. Thus, the sealing capacity of the cement is key, it requires a low permeability, non-shrinking, long durability, ductility and sufficient cement -casing/formation

bonding (Khalifeh & Saasen, 2020a). This study focuses on cement in its liquid state, hence, the cement slurry. The cement slurry is a non-Newtonian fluid with a yield stress. The density may range from 720 kg/m^3 to 2400 kg/m^3 depending on its composition. The rheological properties and the density significantly affect the flow of the cement slurry (Lavrov & Torsæter, 2016b).

2.4.4 Newtonian/ Non-Newtonian models

As previously stated, drilling fluids and cement slurries have non-Newtonian rheology, while the spacer fluids often tend to be Newtonian. In the Newtonian model, the shear stress is linearly correlated to the shear rate, which gives constant proportionality. In Figure 2.4.1 the relationship between the shear stress and shear rate is plotted, where the slope represents the viscosity of the liquid. As the plot is linear, viscosity is considered constant. Thus, viscosity is not affected by fluid motion, but simply by pressure and temperature. In addition, the viscosity and shear rate are independent of each other. This means that the liquid starts flowing once a non-zero shear stress is applied (Çengel et al., 2017). The relationship between shear stress and shear rate is described as:

$$\tau = \mu * \gamma$$

Here, τ denotes shear stress, μ is viscosity while γ is shear rate.

In non-Newtonian models, shear stress is not linearly correlated to shear rate and viscosity is no longer independent of the shear rate. The relationship between shear stress and shear rate is referred to as the apparent viscosity. Fluids for which the apparent viscosity decreases as the rate of deformation increases, are referred to as shear thinning. Fluids that exhibit the opposite behavior is referred to as shear thickening. Most drilling fluids and cements are referred to as shear thinning and is often described by the Bingham Model or the Herschel- Bulkley model (Çengel et al., 2017). The Bingham model can be described as follows:

$$\tau = \tau_y + \mu_p \dot{\gamma}$$

Here, τ denotes shear stress, τ_y is yield point while is μ_p plastic viscosity and $\dot{\gamma}$ is shear rate. Further, the Herschel- Bulkley model can be described as follows:

$$\tau = \tau_0 + k\,\gamma^n$$

Here, τ denotes shear stress, γ is shear rate, k is consistency index and n is the flow index.

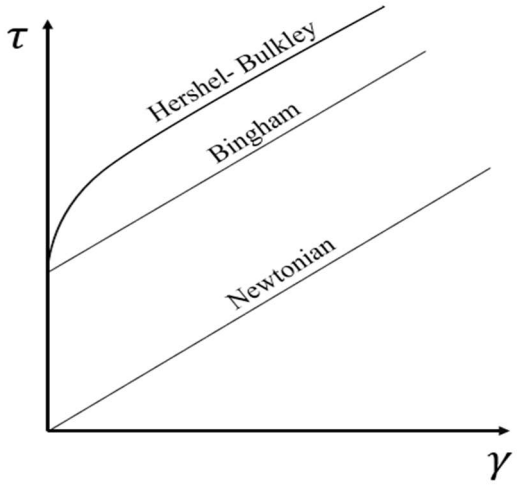

Figure 2.4.1 – Rheology models, where τ denotes shear stress, γ denotes shear rate

2.4.5 Flow Rate and Eccentricity vs. Gravity

In a horizontal annular displacement, there is a competition for the displacement front between flow rate with eccentricity and gravity. Flow rate and eccentricity promotes flow on the wider upper part of the annulus, while gravity forces the fluid flow to stratify at the lower side of the annulus. This results in either 'top side'– or slumping displacement, see Figure 2.4.2. 'Top side' displacement occurs if flow rate and eccentricity is the dominant force. Hence, the higher the flow rate and eccentricity, the more fluid will flow on the wider upper part. If gravity is the dominant force, slumping displacement will occur. Consequently, gravity will strongly promote slumping displacement if there is a considerable density difference between the displacing fluid and displaced fluid (Renteria & Frigaard, 2020). In an ideal displacement, flow rate and eccentricity forces equalize the gravitational force, resulting in a piston like displacement, see Figure 2.4.2.

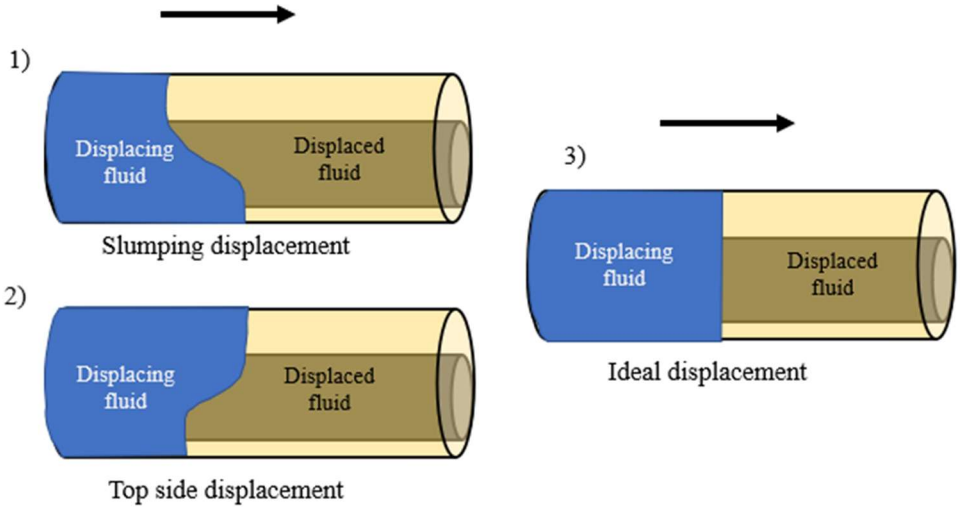

Figure 2.4.2 – Different types of displacement fronts. 1) Slumping displacement, 2) Top side displacement and 3) Ideal displacement

2.4.6 Horizontal Effective Laminar Flow (ELF) guidelines

Fluid design for horizontal wells can be challenging and differs from fluid design for vertical wells. Therefore, to improve and guide fluid design for effective horizontal displacement, a set of guidelines have been developed. Carrasco-Teja (2008) found that, for a horizontal well, steady state displacement cannot be achieved if either of the two following stets of equations are satisfied.

a) $\Delta P_{L,W} < \Delta P_H \; and \; \Delta P_L > \Delta P_{H,N}$

b) $\Delta P_{L,W} > \Delta P_H \; and \; \Delta P_L < \Delta P_{H,N}$

Here delta P_H and P_L respectively denotes the friction pressure drops related with steady laminar flow of the light and heavy fluids in an eccentric annular hole. Delta $P_{H,N}$ is the friction pressure drop corresponding to steady laminar flow of the heavy fluid at the imposed bulk velocity in a concentric annular hole with the gap equal to the narrow gap in the original eccentric annulus. Further, delta $P_{L,W}$ is the friction pressure drop which corresponds to steady laminar flow of the light fluid at the imposed bulk velocity in a concentric annular hole, with the gap equal to the widest gap in the eccentric annular hole (Carrasco-Teja, Frigaard, Seymour, & Storey, 2008).

2.5 Dimensional Analysis of Displacement Efficiency Flows

The prime objective of this thesis is to simulate an actual displacement process from a cementing operation in the field using a laboratory test rig. In order to transfer real operating conditions from the field into the laboratory, a number of equations has been carried out. Specially by using dimensional analysis to reduce the large number complex parameters down to a smaller number of dimensionless groups. For instance, for fluid flow in a cylindrical object (such as a pipe) in which the flow is both incompressible and isothermal (constant temperature and density), the number of relevant variables can be reduced to one. The reduction of parameters can provide a great reward in the way that it will allow a cylinder-model of 1.5 m to yield insight into the dynamics of a full-size cementing operation.
In addition, to simplifying the analysis, that reduction of parameters gives rise to new classes of similarity (Bolster, Hershberger, & Donnelly, 2011). In this thesis geometrical- and dynamic similarity will be used.

2.5.1 Geometric similarity

The model and the full- size structure are geometrical similar when they have the same shape as well as all the linear dimensions must be proportionate and have the same scale ratio, however, the size can differ, see Figure 2.5.1 (Ma, Luo, Thomas Kwan, & Wu, 2019).

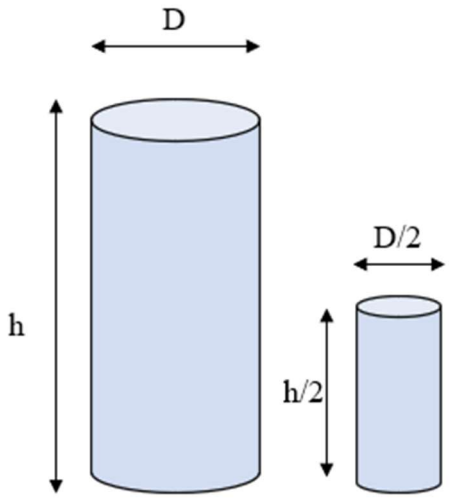

Figure 2.5.1 – Geometric similarity of two cylinders

2.5.2 Dynamic similarity and Governing Equations

Dynamic similarity is the similarity of forces. It is attained when the ratio of the different forces of two geometrically similar vessels are proportionate (Ma et al., 2019). This phenomenon can be used in dimensional analysis to reduce complex long equations that describe the flow into smaller numbers. To model the fluid flow, the general form of the Navier-stokes equations is used. Moreover, the paper 'Advanced Modeling of Cement Displacement Complexities' by Enayatpour and van Oort (2017) is used as a base for the computations for this study. However, with some differences: this study concentrates on flow modeling of Newtonian- and incompressible fluids with laminar flow and isothermal conditions in a circular pipe. The paper by Enayatpour and van Oort (2017), studies 3D flow with both Newtonian and non-Newtonian fluids in a concentric and eccentric annulus. Although the conditions differ somewhat, it acts as a good reference point for the computations for this study (Enayatpour & van Oort, 2017).

The general form of mass- and momentum conservation are given in Eq.1-2:

Mass conservation:

$$\frac{\partial \hat{\rho}}{\partial \hat{t}} + \vec{\nabla}\left(\hat{\rho} \cdot \vec{\hat{v}}\right) = 0 \rightarrow \vec{\nabla} \cdot \vec{\hat{v}}$$

Momentum conservation:

$$\hat{\rho}_i \frac{\partial \vec{\hat{v}}}{\partial \hat{t}} + \hat{\rho}_i \left(\vec{\hat{v}} \cdot \vec{\nabla}\right) \vec{\hat{v}} = -\vec{\hat{\Delta}}\hat{p} + \hat{\mu}\, \vec{\nabla^2}\, \vec{\hat{v}} + \hat{\rho}_i \vec{\hat{g}}$$

Where $\hat{\rho}$ is density, $\hat{t}$ is time, $\vec{\hat{v}}$ is fluid velocity vector, $\hat{p}$ is fluid pressure, $\hat{\mu}$ is fluid viscosity and $\vec{\hat{g}}$ is acceleration of gravity.

To achieve a dimensionless set of variables, an appropriate characteristic flow velocity, density and length is chosen. Further, a dimensionless length x, time t, velocity and pressure can be introduced:

$$\vec{\hat{v}} = \widehat{v^*} \cdot \vec{v}\,, \qquad \hat{p} = \widehat{p^*} \cdot p, \qquad \vec{\hat{\nabla}} = \frac{1}{\widehat{D_H{}^*}}, \qquad At = \frac{\hat{\rho}_1 - \hat{\rho}_2}{\hat{\rho}_1 + \hat{\rho}_2}, \qquad \hat{t} = \frac{\widehat{D_H{}^*}}{\widehat{v^*}},$$

$$\hat{\rho}_i = \hat{\rho}\,(1 + \Phi_i \cdot At) \rightarrow \Phi_i \begin{Bmatrix} +1 \,|\, i = 1 \\ -1 \,|\, i = 2 \end{Bmatrix}$$

Where $\widehat{D_H}^*$ denotes the hydraulic diameter, $\widehat{v^*}$ characteristic velocity of fluid, At is Atwood number.

Adding the above listed variables to the Navier- Stokes equation, the equation then becomes:

$$\hat{\rho}\ (1+\Phi_i\cdot At)\ \frac{\widehat{v^{*2}}}{\widehat{D_H}^*}\left(\frac{\partial\vec{v}}{\partial \mathrm{t}}+\left(\vec{v}\cdot\vec{\nabla}\right)\vec{v}\right)=\ \frac{\widehat{p^*}}{\widehat{D_H}^*}\ \vec{\nabla}p+\frac{\hat{\mu}\widehat{v^*}}{{D_H}^{*2}}\ \nabla^2\vec{u}+\hat{\rho}\,(1+\Phi_i\cdot At)\hat{g}$$

To simplify, the equation is multiplied by $\frac{{D_H}^{*2}}{\hat{\mu}\widehat{U^*}}$, the equation then becomes:

$$(1+\Phi_i\cdot At)\ \frac{\hat{\rho}\,\hat{g}D_H^{*2}}{\hat{\mu}\widehat{v^*}}\left(\frac{\partial\vec{v}}{\partial \mathrm{t}}+\left(\vec{v}\cdot\vec{\nabla}\right)\vec{v}\right)=\ -\frac{\widehat{\rho^*}\,\widehat{D_H}^*}{\hat{\mu}\,\widehat{v^*}}\ \vec{\nabla}p+\nabla^2\vec{v}+\ (1+\Phi_i\cdot At)\frac{\hat{\rho}\ \hat{g}\ \widehat{D_H}^*}{\hat{\mu}\widehat{v^*}}$$

$$=\frac{\hat{\rho}\ \widehat{v^*}\widehat{D_H}^*}{\hat{\mu}}\cdot\frac{At\ \hat{g}\ {D_H}^*}{\widehat{v^{*2}}}$$

$\frac{\hat{\rho}\ \widehat{v^*}\widehat{D_H}^*}{\hat{\mu}}=Re$ and $\frac{At\ \hat{g}\ {D_H}^*}{\widehat{v^{*2}}}=\frac{1}{Fr^2}$, thus the final equation becomes: $=\frac{Re}{Fr^2}$

Where $\frac{\hat{\rho}\ \widehat{v^*}\widehat{D_H}^*}{\hat{\mu}}$ = Reynolds number, $\frac{\hat{\rho}_1-\hat{\rho}_2}{\hat{\rho}_1+\hat{\rho}_2}$, = Atwood number and $\sqrt{\frac{\widehat{v^{*2}}}{At\ \hat{g}\ {D_H}^*}}$ = Froude number
The change to dimensionless variable does not only provide a superficial simplification of the equation, but also greatly reduces the work needed to study the flow. Now, the flow characteristics such as Reynolds number, Froude number and Atwood number can be studied by investigating the effects of varying velocity, viscosity, and density.

Atwood Number is a dimensionless parameter which is associated with hydrodynamic instabilities in density stratified flow. It describes the density ratio of the sinking or rising fluid due to respectively, gravitational- or buoyancy effects, where p1> p2. It defines the difference in density between the heavy fluid p1, and the light fluid, p2, divided by the total sum of the density of the fluids (Youngs, 1991).

Atwood number $=\ \frac{\hat{\rho}_1-\hat{\rho}_2}{\hat{\rho}_1+\hat{\rho}_2}$,

The Reynolds number is the dimensionless parameter which corelates the ratio of the internal- and viscous forces. It is used to determine whether the flow is laminar, turbulent of transient, where the effect of viscosity is an important parameter in controlling the flow velocity (Rehm & International Association of Drilling, 2008). The Reynolds number is defined as

$$\text{Reynolds number} = \frac{\hat{\rho}\ \widehat{U^*}\widehat{D_H{}^*}}{\hat{\mu}}$$

The Froude number is the dimensionless parameter which describes the ratio of inertia forces and the gravitational forces. It is used to indicate whether the inertia terms dominate over the gravitational effects. If the velocity in the fluid is very high, the gravitational forces can be neglected, for this case, the Froude number would be very high (Rapp, 2017). For full-size cementing operations the Froude number tends to be quite low (Fr= 0.3-2). The Froude number is defined as:

$$\text{Froude number} = \sqrt{\frac{\widehat{U^{*2}}}{At\ \hat{g}\ D_H{}^*}}$$

These three dimensionless parameters allow full-size operations to be correlated with small model experiments. If a Froude number of e.g. Fr= 0.5 is obtained for both the full-size and the small model, one can conclude that the ratio of forces is the same for both the full-size and the laboratory experiment. The same conclusion can be drawn for the other dimensionless numbers. However, it is not possible to satisfy the similarity requirements posed by Reynolds, Froude and Atwood number simultaneously. Therefore, it is necessary to determine which is the dominant force according to which the scaling must be done. In this thesis, the Froude number and Reynolds number have been decided as the dominant forces.

2.6 Previous Research

First, a general overview of previous research in form of laboratory- and full- scale experiments, including Computational Flow Dynamics (CFD)- simulations is presented. Furthermore, more important and specific research has been provided in accordance with the thesis topic. This includes guideline, laboratory experiments and CFD simulations. Finally, casing rotation/vibration research is discussed.

2.6.1 General Overview

Tehrani et al. (1992) investigated both theoretically and experimentally effect of eccentricity on displacement efficiency in inclined wells. The prerequisites of the study was: Laminar displacement for non-Newtonian fluids in an 3D annular space. It was concluded that centralization of tubing, high density contrast between the drilling fluid and cement and a positive rheological hierarchy is required. In addition, the study showed that inclination decreased with the gravitational effect of the fluid displacement. This will reduce the effect of the density contrast between the drilling fluid and the cement, and thus, inclination will have an adverse effect on the displacement efficiency (Tehrani, Ferguson, & Bittleston, 1992).

Jakobsen et al. (1991), studied the effect of steady fluid displacement with different densities in an 55 % eccentric inclined well (60 degrees). Through laboratory experiments, they found that if the displacing fluid was 5 % heavier than the displaced fluid, the lighter fluid will flow from the narrow area into the wider upper area of the annulus. This mechanism, the buoyancy-induced process, will greatly improve fluid displacement (Jakobsen et al., 1991).

Malekmohammadi et al. (2010), studied displacement flow of two miscible fluids in a laminar fluid flow in an eccentric vertical well. They determined that it is possible to achieve a steady traveling displacement front in an eccentric annulus, even when strongly eccentric. According to Malekmohammadi et al., a steady displacement is desired over an unstable one. The study indicated they could achieve a steady displacement when having strong eccentricity combined with slower flow rate and a positive ratio of density and viscosity. Additionally, they also discovered that in a steady displacement, eccentricity stimulates a secondary azimuthal counter-current flow both below and above the adverting fluid interface. This fluid flow drives the displacing fluid over to the wide side of the annulus, resulting in an advancing

spike of displacing fluid, leaving an elongation spike of displacing fluid on the narrow side (Figure 2.6.1) (Malekmohammadi, Carrasco-Teja, Storey, Frigaard, & Martinez, 2010).

Figure 2.6.1 – Displaying a typical result of Malekmohammadi et al. The black color represents the displacing fluid, while the transparent fluid represents the displaced fluid. An elongated spike on the left side caused by eccentricity is illustrated.

In 2019, Skadsem & Kragset (2019) studied displacement in an irregular and regular eccentric annulus to investigate the effect of buoyancy and inertia on viscoplastic fluids. In the numerical analysis, they also compared their results with the vertical Effective Laminar Flow (ELF) guidelines presented by Couturier et al. (It should be noted that vertical ELF works as a "rule of thumb" in the industry, involving density-, viscosity- and friction pressure hierarchy.) (Couturier, Guillot, Hendriks, & Callet, 1990). In the study done by Etrati and Frigaard (2019), numerous numerical 3D simulation of laminar flow of miscible fluids of a vertical, narrow and eccentric annulus was carried out. The results showed qualitive agreement with the experiments performed earlier by Skadsem & Kragset (2019) .

Aas et al. (2016) conducted full-scale testing to evaluate the quality and sealing ability of a cement placement when tubing is left in hole with an eccentric annulus. The test assembly were inclined to 85°, thus, approximately horizontal. The experiments showed that it is possible to obtain good cement quality also when tubing is left in hole. They concluded that there was a complete displacement of displaced fluid and full cement coverage, except for some minor micro annuli. It was also determined that it was favorable for the displacement to have a light, not dense, brine being displaced by a much denser cement. However, it should be noted that the test was performed at highly optimal conditions, with slow pumping rates and

minimal contamination. Nevertheless, it serves as a good indication on how the displacement will work at for full-scale operations (Aas et al., 2016).

In all above mentioned experiments and surveys, displacing fluid in an eccentric geometry favors flow on the wider part of the annulus where also azimuthal flow can be detected. It is also known that mobilization of fluid in the lower narrow side of the annulus will favor fluid flow and thus optimize displacement efficiency.

2.6.2 Horizontal Eccentric Annuli Research

A publication considering viscoplastic horizontal fluid displacement in an eccentric and narrow annulus, was presented by Carrasco-Teja in 2008. A horizontal, narrow and eccentric displacement with laminar flow, was considered in the study. Interestingly, it was found that not buoyancy as previously assumed, but the competition between eccentricity and fluid rheologies was the determining factor of horizontal displacement. They also commented that the buoyancy does contribute to determine the axial length of the steady- state flow profile. In this study, Carrasco-Teja also presented a set of horizontal Effective Laminar Flow (ELF) conditions. It was concluded that in order to ensure steady- state displacement, these conditions must not be fulfilled, see section 2.3 Fluid Design (Carrasco-Teja et al., 2008).

To follow up this research, Skadsem et al. (2019) investigated the above-mentioned guidelines from Carrasco-Teja using 3D CFD simulators of full-scale experiments. They observed that, the two criteria were not satisfied, and it was concluded that steady laminar flow exist as reported by Carrasco-Teja in the former study. It should be noted nevertheless, that the CFD simulations indicated that steady-state displacement only exists for long test assemblies. For short test assemblies, steady-state displacement could not be observed (Skadsem, Kragset, & Sørbø, 2019).

Renteria & Frigaard (2020) carried out ≈ 300 laboratory experiments of miscible Newtonian displacement flow. They studied horizontal displacement efficiency by varying density difference, viscosity, eccentricity and laminar Reynolds numbers. The experimental results were compared to the calculations in Carrasco-Teja's (2008) model. Renteria & Frigaard found that their results were completely in line in terms of prediction of underlying competition between eccentricity and buoyancy (Renteria & Frigaard, 2020).

The studies and experiments as described herein, all concludes that for long horizontal annuli, buoyancy drives a stable stratification front of the displacement flow, which is beneficial to the displacement efficiency. Contrarily, eccentricity influence the fluids to move faster on the wider, upper part, thus, acts detrimental to efficient steady-state displacement.

2.6.3 Casing/ Tubing Rotation- and Vibration Research

Utilizing vibration as a form of creating oscillations, axial and lateral waves is a fairly new method in the industry. Hence, not a lot of research can be found, but, casing rotation and reciprocation (especially rotation) may provide some insight into the same mechanisms as for vibration. Therefore, previous research of casing rotation and reciprocation may be useful in the understanding of casing vibration.

S.R Keller et. al. (1987) performed full-scale experimental tests on both impermeable and permeable deviated wellbores of 80° (from vertical). The objective was to investigate whether rotation and reciprocation would improve displacement efficiency. Multiple test- scenarios were performed and it was concluded that pipe rotation and reciprocation could significantly increase displacement efficiency of settling drilling fluid in inclined wells (Keller et al., 1987).

Bu et. al. (2018) numerically simulated the influence of eccentricity and density differences on a highly deviated well. In the simulations, they varied the density difference and thereby changing the buoyancy force. The density differences varied from -100 kg/m^3 to 700 kg/m^3 and it was concluded that density difference improved displacement efficiency if the density difference is less than 600 kg/m^3. Although, the eccentricity was set to below 20% (from concentric) a slight improvement of the displacement efficiency could be detected, but as the eccentricity increased to more than 20%, it was drastically reduced. Figure 2.6.2 displays the results from the simulation of eccentricity with and without rotation. Further, casing rotation showed to greatly improve the displacement efficiency. They found that as casing rotation increased within a specific range, the more circumferential spiral flow forms, and hence, leads to improved displacement efficiency.(Bu et al., 2018)

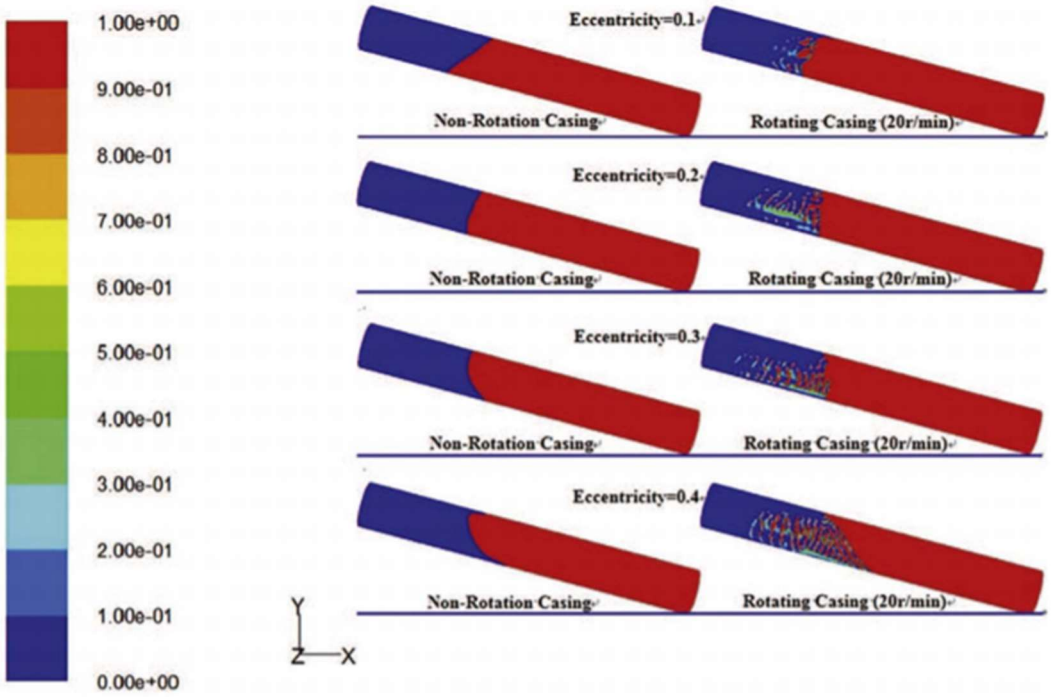

Figure 2.6.2 – Simulation results of eccentricity with and without casing rotation of Bu et. al. (2018). Blue color represents displaced fluid and red represents displacing fluid.

One of the few publications with regards to vibration, Thom et. al. (2016) performed a field study for abandonment of rig-less subsea wells in the North Sea. A vibration tool that produce oscillation waves in the flow, was installed inside the production tubing to increase cement coverage in the annulus and improve displacement efficiency. Even though there was no detailed description regarding the effect of the tool presented in the 2016 paper, it was stated as an advantageous addition to the process, especially for breaking down high gel strengths found in older drilling fluid left behind from drilling the well. Vibration enabled the drilling fluid to be mobilized, resulting in a decreased gel strength (Thom et al., 2020).

Based on available research regarding casing/tubing movement and displacement of fluids as presented here; experiments from laboratory to CFD simulations and field studies, all show that pipe movement on displacement efficiency, in all aspects are beneficial.

3 Methodology

Before the experimental set up is described, an overview of the field settings the experiments are attempting to simulate, in addition, the dimensional analysis is discussed.

For annular displacement, the process starts at the bottom of the well and proceeds upwards. Therefore, it is natural that the horizontal section is the starting point for the displacement. Cement is pumped down the tubing and through punched holes/ cut tubing into the annulus. Packers are installed to act as a barrier in the annular space, as well as preventing cement contamination by reservoir fluids. For the same reason, a bridge plug is placed inside the tubing below the circulation point, see Figure 3.1.
In the horizontal section for TTA wells, the tubing/liner to be cemented would commonly have an outer diameter of 3.5 – 5.5 inches (88.9 – 139.7 mm). The casing in this section is the production casing which would typically have an outer diameter of 7.625 – 9.625 inches (193.7 – 244.5 mm). This leaves an annular gap, also referred to as the hydraulic diameter, of 4.124 inches (104.8 mm).

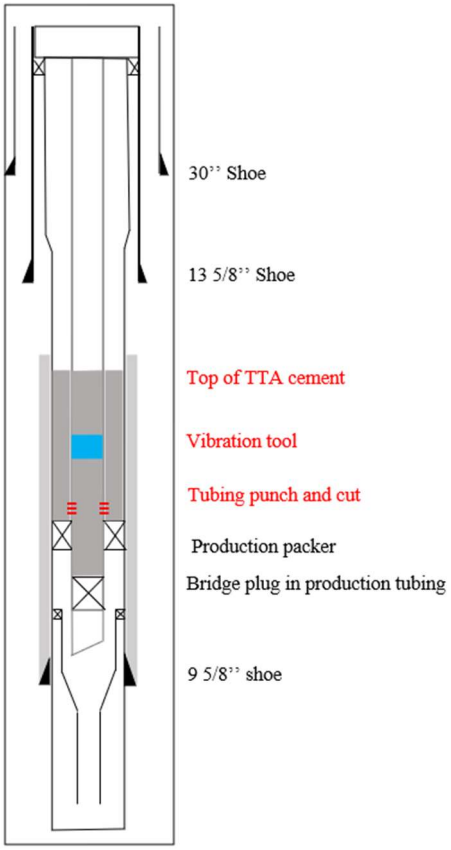

Figure 3.1 – Well Schematic of a TTA cement operation. This is an original Figure that is based on the figure from Thom, F. et. Al (2020).

3.1 Dimensional analysis and Limitations

The prime objective of this thesis is to simulate an actual displacement process from a cementing operation in the field using a laboratory test rig. To achieve this, dimensional analysis is used. Further, field condition parameters such as well geometry, flow rate, densities and viscosities of displacing- and displaced fluid have been provided. However, when performing experimental investigations, there will always be some limitations to take into consideration. For instance, the test rig has a relatively shot test section. Therefore, is not functionally appropriate to use high flow rates for these experiments. Furthermore, this thesis considers Newtonian fluid displacement. This limits the possibility of achieving very high densities/viscosities. Without the use of polymers (and thus making the fluid non-Newtonian), it is fairly difficult to obtain high viscosities and densities. These limitations have been considered for the dimensional analysis.

3.1.1 Dynamic similarity

In Chapter 3.4 the dimensional analysis of the displacement flow of two Newtonian fluids were conducted. Considering dynamic similarity, three non-dimensional parameters were derived: Atwood number, Reynolds number and Froude number. As mentioned, it is not possible to satisfy all three parameters (Reynolds-, Froude- and Atwood number) simultaneously. In this study, the internal forces have been found to be the dominant forces, thus Froude- and Reynolds number is used for the dynamic similarity.
Data obtained from the field, show that the Froude number generally ranges from 0.55 –1.73 and Reynolds number ranges from 462 – 657 (Table 3.2). To obtain Froude- and Reynolds similarity, flow rate and viscosities/densities of the displacing and displaced fluid have been investigated and varied. Eventually, a Froude- and Reynolds number for the test rig of respectively 0.541 and 426 was achieved, see Table 3.2. This results in a very good dynamic similarity considering the above mentioned limitations.

3.1.2 Geometric similarity

In the geometrical scaling, different geometrical similarities and relations from field conditions were considered, see Tables 3.1-3.2. In the field data provided, casing sizes varied from $9^{5/8}$ – $7^{5/8}$ inches and tubing sizes from $5^{1/2}$ – $3^{1/2}$ inches. This gives a range of relations of 1.39 to 2.18. For the laboratory test rig, the outer pipe has an outer diameter of 70 mm, while the inner pipe has an outer diameter of 50.5 mm. This gives a relation of 1.39. Table

3.1 lists ratio, Froude- and Reynolds number. As shown in Table 3.2, the geometrical relation of the test rig and Case 3 is perfectly similar. However, to achieve a satisfactory dynamic similarity analysis, Froude- and Reynolds similarity is necessary. Therefore, due to good Froude- and Reynolds similarity, Case 2 was selected for further investigation. Although the test rig and Case 2 is not perfectly alike, the geometrical similarity is not entirely unsatisfactory. The geometrical difference between the two is approximately 25%.

Table 3.1 Geometric dimensions for the test rig

Parameter	Symbol	Value
Inner pipe diameter	ID	70 mm
Outer pipe diameter	OD	50.5 mm
Hydraulic diameter	D_h = ID – OD	19.5 mm
Total test section length	L	1.516 m

Table 3.2 Geometric and Dynamic relations between the test rig and field values

	OD Casing	OD tubing	Ratio	Froude Number of cement slurry	Reynolds Number of cement slurry
Case 1 (field)	7.625 inches	3.5 inches	2.18	0.757	657
Case 2 (field)	9.625 inches	5.5 inches	1.75	0.557	483
Case 3 (field)	7.625 inches	5.5 inches	1.39	1.736	556
Test rig (model)	70 mm	50.5 mm	1.39	0.541	462

3.2 Fluid design

The fluids are designed according to the dimensional analysis. For the purpose of simplicity, fresh water was selected as the base for both test fluids. It is an incompressible, Newtonian fluid with a low and constant viscosity, in addition to be a good solvent for salt and sugar

weight agents. The density of the displacing fluid was achieved using dissolved sucrose. A black ink is added to create a visual contrast between the fluids. NaCl (salt) was then added for the purpose of measuring conductivity. A test was performed to determine if the black ink would affect the density of the fluid. But the test showed that the black ink had little or no effect on the density. Table 3.3 shows the parameters selected for the experimental study.

Table 3.3 Design parameters for the experiments

Fluid	Color	Density	Viscosity	Flow velocity
Displacing fluid	Black	1111 kg/m^3	2.5 mPa*s	6 l/min
Displaced fluid	Transparent	998 kg/m^3	1 mPa*s	6 l/min

*See Appendix C for calculation of weighing material (glucose) for achieved density of displacing fluid.

3.3 Experimental setup

Figure 3.2 illustrates the schematic representation of the flow loop and Figure 3.3 shows the test rig in both its vertical and horizontal position. It consists of an outer pipe with an inner diameter of 70 mm and an inner pipe with an outer diameter of 50.5 m. The outer pipe is a transparent pipe made of Lexan, while the inner pipe is made of steel. An eccentricity device is mounted on the test rig, this devise allows the inner pipe to be adjusted relative to the fixed outer pipe. The eccentricity of the inner pipe can be set anywhere from concentric to completely eccentric (resting on either the top or bottom of the outer pipe). It is measured by depth gauges mounted on the bottom-assembly of the rig. The experimental setup also consists of a positive displacement pump which supplies the annulus with fluid at a constant rate. The flow rate is controlled by a variable frequency driver (VFD) and measured by an electromagnetic flow meter. At the annulus outlet, a conductivity meter is installed to measure the amount of salt in the fluid. The general dimensions of the test rig are listed in table (1).

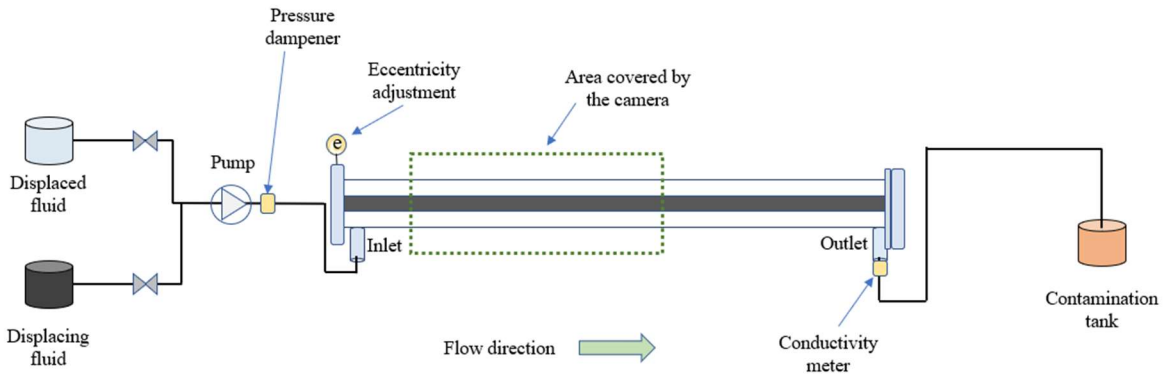

Figure 3.2 – Schematic of experimental set

Figure 3.3 – Pictures of the test rig, both in vertical and horizontal position.

3.3.1 Displacement visualization

The main method used for analysis in this study is direct flow visualization. Therefore, to establish a significant visual contrast between the displaced fluid and the displacing fluid, a

non-waterproof black ink was added to the displacing fluid, while the displacing fluid was kept transparent. Additionally, black curtains was installed around the rig to secure consistent lighting conditions by eliminating light pollution.

3.3.2 Density and viscosity measurement

Density of the displaced and displacing fluid was measured using a Density meter DMA 4100 M, which uses the oscillating U-tube method. A fluid sample was inserted into a U-tube glass and vibrated at a characteristic frequency to determine the fluid density.

Viscosity of the displacing and displaced fluid was measured using a Physica MCR 301 rheometer. The fluid sample was placed between two plates where the bottom plate rotates at a fixed speed. The top plate measured the torsional force produced in the fluid sample and the stress- strain relationship was found. As a result, the viscosity was determined.

3.3.3 Flow Meter

Due to a malfunctioning flow meter, manual testing of the flow rate had to be performed. The pump was set to a desired position (ca 1.1 % of capacity), a 2 liter measuring cup was used for volume measurement. A timer was activated when the liquid started to fill up the cup and stopped once the volume of 2 liter was reached. After 20 seconds, the measuring cup was filled up, and the flow rate calculated to 6 l/min. This procedure was repeated 3 times to ensure correct time measurements.

3.3.4 Pump

A Verderflex Rollit 25 pump was used to pump the test fluids from the fluid storage tanks to the test rig annulus. The pump has a max flow rate of 2500 l/min, a max pump speed of 165 RPM and a maximum discharge pressure of 4 bar (Verder-Liquids, 2021).

3.3.5 Conductivity Meter

To measure the conductivity of the fluids a Jumo CTI - 500 was used placing the probe inside the outlet pipe, see Figure 3.2. The device was connected to a PC with a software program

displaing the measured conductivity on the y- axis and the corresponding time on the x- axis (JUMO, 2021).

3.3.6 Eccentricity adjustment

The pipe can be adjusted from fully concentric (0% eccentricity) to approximately 100 % eccentric. Alterations to eccentricity are made by regulating two screws which supports the inner pipe. The screws are regulated on an angle disc containing both angles and corresponding length measurements in mm (from 0-9 mm). The desired eccentricity was maintained throughout the test section. The eccentricity is symmetrical about the vertical axis passing through the annulus from 0° to 180°, which respectively denotes 0% eccentricity and 100% eccentricity. For instance, to obtain an eccentricity of 56.25 degree, the screws must be moved to 8 mm where the length measurement corresponds to 56.25°, see Figure 3.4.

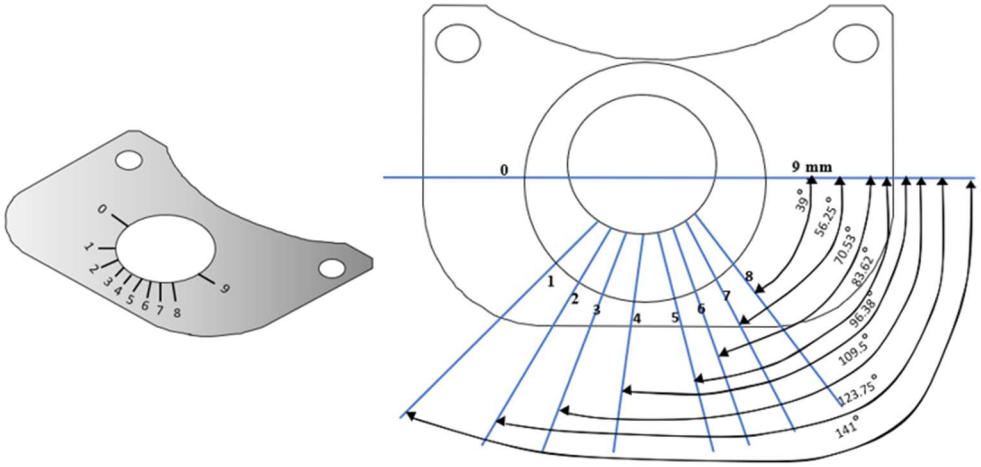

Figure 3.4 – Eccentricity adjustment

3.4 Computer Image Analysis

The main method for analyzing the displacement front is by direct flow visualization. Therefore, an image analysis program was created by using python, a high-level general purpose programming language. The task of this image-analysis program is to locate the interface of displacing and displaced fluid to produce an image of solely the edges of the displacement front. This image analysis program was used as a secondary verification method.

The program records convert the image pixel values into greyscale, ranging from 0 (black) to 255 (white). After the conversion, a median filter was applied to the image to reduce some of the light reflection. A threshold value was then selected and set manually to remove anything in the image which was not desired. The undesired area was then set to 255 (white), whereas the desired area was set to 0 (black). The threshold value for this analysis ranges between 40 to 110, depending on the amount of light in the image. Finally, the entire black displacing fluid was detected, as we wish to only study the edges of the displacement front, a new area-specific threshold was set where the edges was set to a lime green color. The lime green color was chosen for a better contrast to the black displacement fluid.

3.5 Experimental plan

In Table 3.4 the experimental plan is presented. Due to extreme time constraints, the experiments focuses on investigating the effects of eccentricity and vibration. Flow rate, density and viscosity of both the displaced fluid and the displacing fluid was kept constant. Eccentricity was investigated at three stages: concentric (0 % eccentricity), moderately eccentric (46 % eccentricity) and extreme eccentricity (92 % eccentricity). Vibration was applied to these three stages simultaneously. Four different intensities was used to study the effect: none (0%), low (15%), medium (30%) and high (65%).

Table 3.4 Experimental series

series	Density, Displaced	Density, Displacing	Viscosity, Displaced	Viscosity Displacing	Flow rate	Vibration intensity	Eccentricity
1	998 kg/m^3	1111 kg/m^3	1 mPa*s	2.5 mPa*s	6 l/m	2.48 Hz, 4.95 Hz and 10.73 Hz	0 %
2	998 kg/m^3	1111 kg/m^3	1 mPa*s	2.5 mPa*s	6 l/m	2.48 Hz, 4.95 Hz and 10.73 Hz	46%
3	998 kg/m^3	1111 kg/m^3	1 mPa*s	2.5 mPa*s	6 l/m	2.48 Hz, 4.95 Hz and 10.73 Hz	92%

3.6 Test procedure

Prior to start-up testing, the test fluids was prepared and kept in two separate tanks, then a small liquid sample from each tank was obtained to check the properties. To measure the densities, an electrical densitometer was used while a Malvern rheometer was used to measure the viscosities. Further, the eccentricity device was adjusted to the desired eccentricity (e.g. 98% eccentric) and the fluid to be displaced pumped into the annulus. For experiments with vibrations, the vibration toll was now activated, and the two-way valve switched from displaced to displacing fluid. The camara was set to record displacing fluid enter the test section. The conductivity meter at the outlet was continuously measuring the fluid outflow conductivity. When the displacing fluid reaches the conductivity meter the pumped was stopped and the experiment concluded. To prepare for the next experiment, the black displacing fluid was then (to some degree) pumped back into the tank to be reused. The valve on the pump was switched back to the transparent displaced fluid and the test section refilled.

4 Results and Discussion

The laboratory set up in section 4.2 was applied to investigate the effect of eccentricity and vibration on a displacement process. The experiments was divided into three experimental series. Serie 1 investigates the effect of vibration on a concentric annulus (0 % eccentricity), while Serie 2 investigates the effect of vibration on a 46 % eccentric annulus. Finally, Serie 3 investigates the effect of vibration on a 92 % eccentric annulus. In the following chapter, the different forces acting on the system will be taken into consideration and discussed. It should be noted that in some of the pictures black sealing paste can be seen. The paste is smeared on the inside of the pipe and does not significantly affect the displacement flow but is marked with a pink arrow (Figure 4.1 - 12 sec).

A computer image analysis program created with by using python was developed to locate the interface of the displacing and displaced fluid. Subsequently the analysis program produce an image of the edges of the displacement front. The analysis program acts as a secondary verification method. It is especially useful to locate the edges of the displacement front where the displacement process was nearly completed, where it is difficult to detect the edges visually. Although most images were analyzed acceptably, few of the images had some defaulting in their analysis.

For this reason, the pictures where it is difficult to detect the edges visually, is added below the original image, to help identify the interface between the fluids. All analyzed images can be found in Appendix B.

4.1 A typical displacement

Before presenting the result of the different series of experiments, a typical test result is given. Figure 4.1 shows typical images of the displacement process presented at different times. For this purpose, a displacement with an eccentricity = 46 % and vibration = 4.95 Hz (moderate vibration) has been chosen. From the images, the first observation to be made is that although the fluids both are miscible, the bulk of the two different fluids remains separate and rather unmixed. However, the interface of the fluids are slightly diffused, and some degree of mixing is observed, but no evidence of large-scale mixing. The observed diffusion can probably be explained by the velocity change at the inlet of the annulus. The flow must change its path from lateral to horizontal at the inlet which can create a turbulence in the flow,

and thus, some diffusion is seen. The shape of the interface elongates at the narrow lower part of the annulus, and a characteristic distinct ‘spike’ is observed. This characteristic spike on the lower narrow side of the annulus is observed throughout the experiments, with the exception of one experiment. This experiment will be discussed further in section 4.3 Serie 3 – strong eccentricity.

4.1.1 General displacement profile

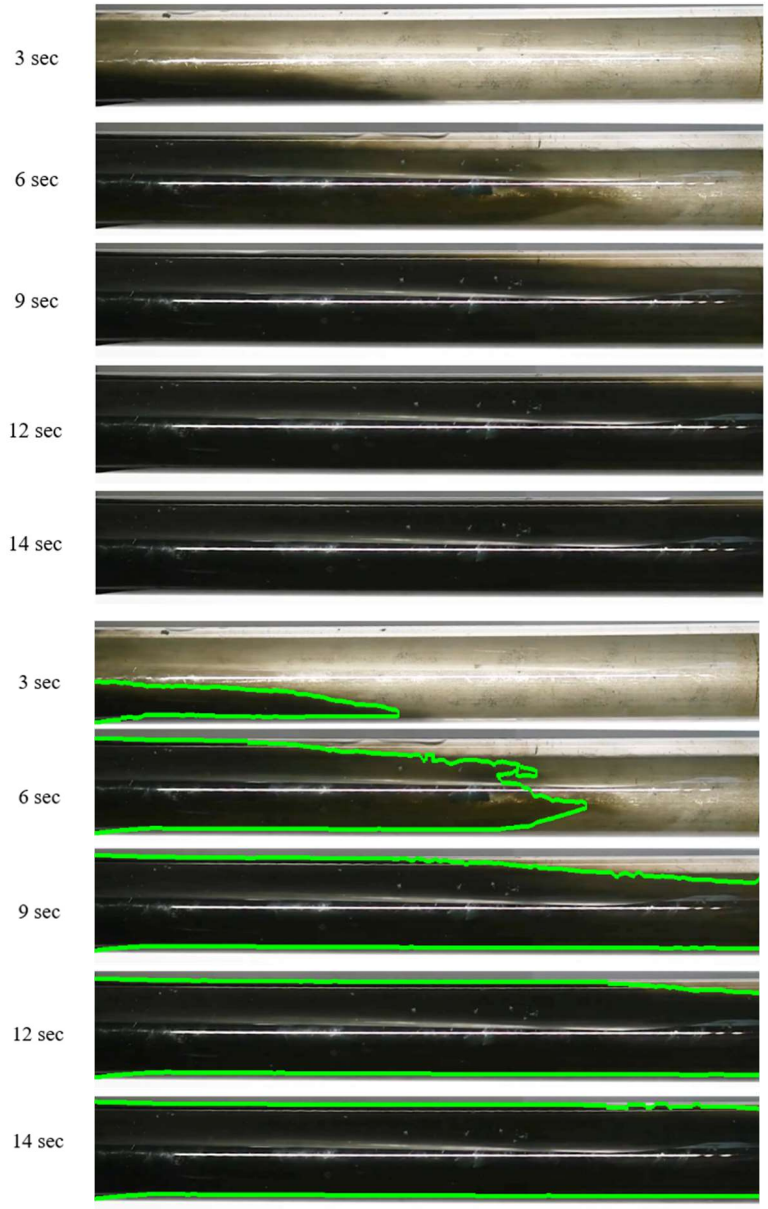

Figure 4.1 – A typical displacement time lapse. Eccentricity = 46 % (moderate), vibration = 2.48 Hz (low). In addition, the computer image analyzed image is included to better help detect the interface of the fluids.

The general displacement profile in the experiments elongates at the lower narrow side of the annulus, see Figure 4.1. This displacement profile can be described by the counteraction between gravity and eccentricity. In section 3.1.4 Gravity vs. Eccentricity, a description of two different displacement fronts are given, ‘top side’- and ‘slumping’ displacement. The general behavior observed was slumping displacement. The slumping displacement profile is a result of the counteraction between the combination of flow rate and eccentricity and gravity, where gravity is the dominant force in this system. Thus, fluid will flow on the lower side of the annulus.

4.2 Effect of eccentricity.

In this section the effect of eccentricity on the displacement efficiency is studied. The results are presented as a series of pictures comparing the displacement fronts of the different runs. Figure 4.2 displays respectively the series next to each other in three columns: zero eccentricity (0%), moderate eccentricity (46 %) and strong eccentricity (92 %). Flow rate, densities and viscosities are kept constant. To investigate the effect of eccentricity isolated, vibration is set to zero.

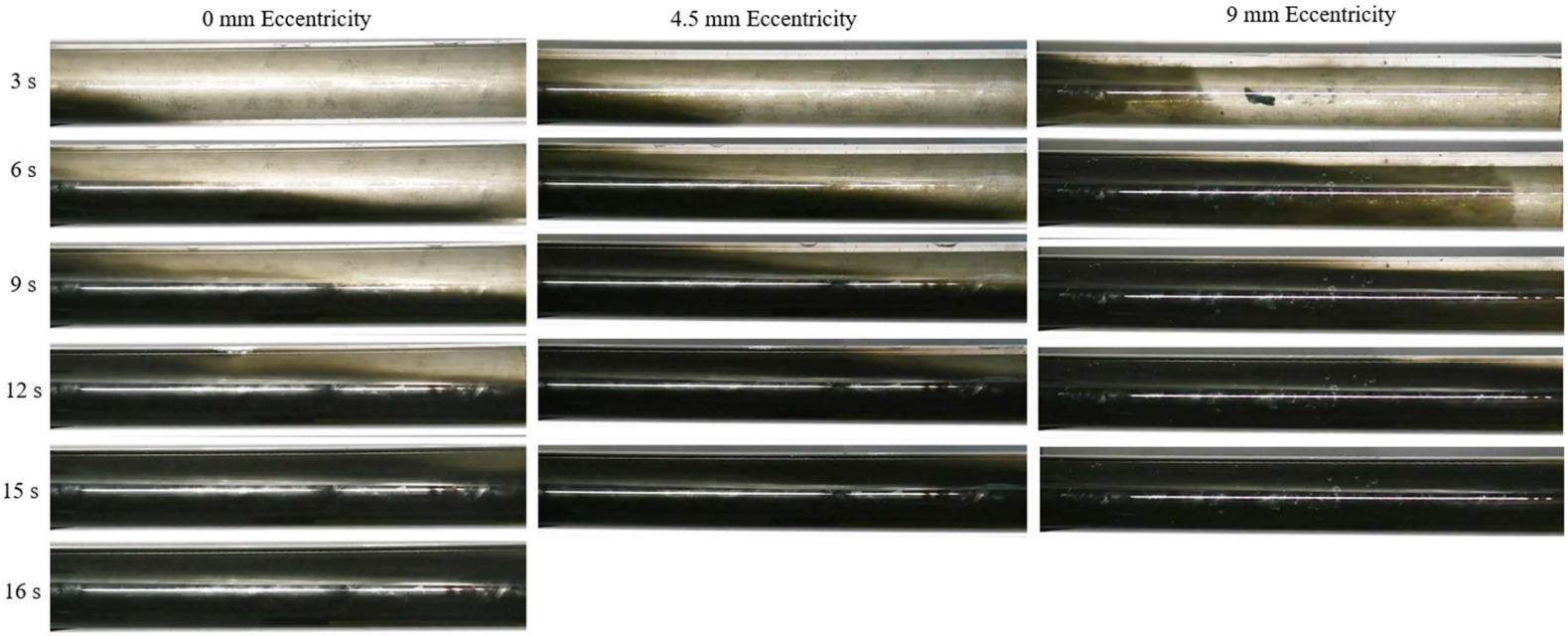

Figure 4.2 – Displacement fronts of the three series: no eccentricity (0 %), moderate eccentricity (46 %) and strong eccentricity (92 %) at the same time lapse.

Figure 4.3 shows the displacement of 0 %, 46 % and 92 % eccentricity at time = 3 seconds. The displacement front is clearly affected by the eccentricity. The front in 0 % eccentricity has moved less compared to eccentricity of 46 % and 92 %. Moreover, as eccentricity increases, the black displacing fluid is distributed more uniformly in the annulus. Thus, the front elongates less at the bottom with increasing eccentricity.

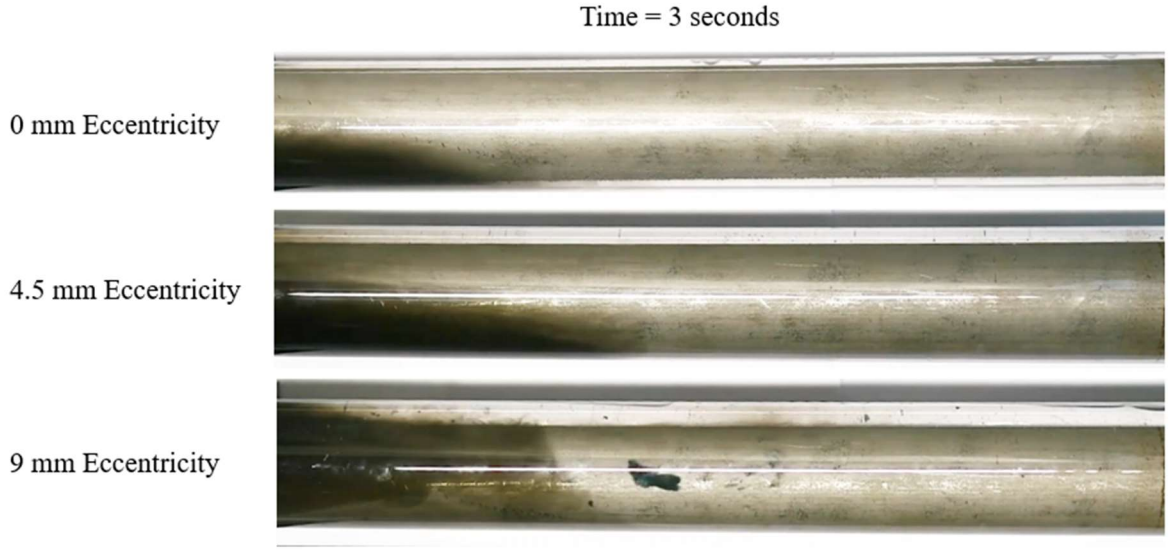

Figure 4.3 – Displacement fronts of 0 %, 46 % and 92 % eccentricity at time = 3 seconds.

Figure 4.4 displays the front of 0 %, 46 % and 92 % eccentricity at time = 6 seconds. Comparing time = 3 seconds to 6 seconds, the effect of eccentricity is still apparent. The front observed in 0 % eccentricity is further elongated along the bottom of the annulus, while the more eccentric annuli has a more uniform displacement front. 92 % eccentricity promotes especially a piston like front. However, there is a noticeable spike of undisplaced transparent fluid in the upper part of the annuli.

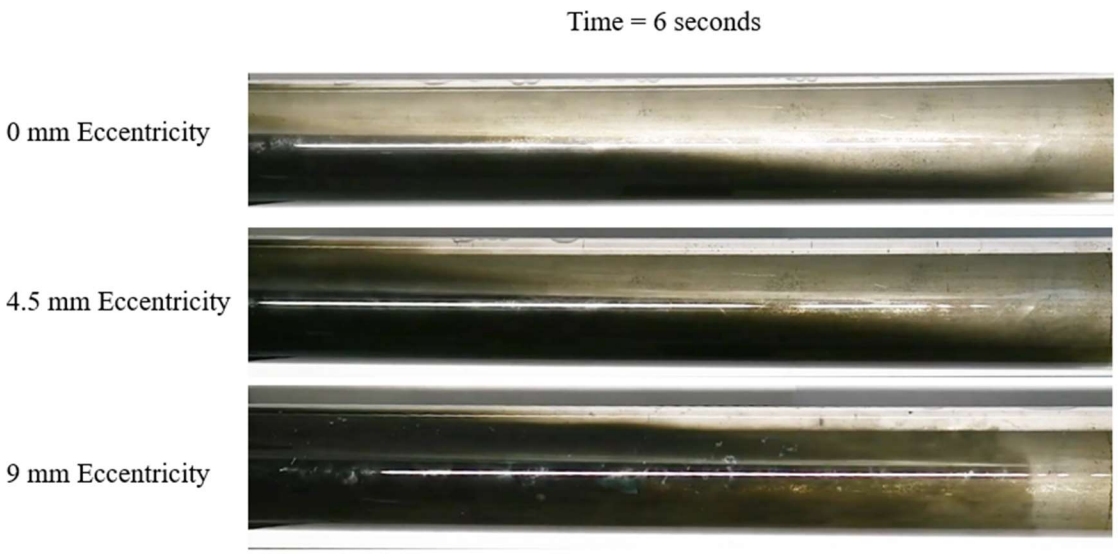

Figure 4.4 – Displacement fronts of 0 %, 46 % and 92 % eccentricity at time = 6 seconds.

Figure 4.5 show the front of 0 %, 46 % and 92 % eccentricity at time = 12 seconds. As shown, the displacement process is almost completed for the 46 % and 92 % eccentricity runs. The red arrow indicates where some transparent fluid is still undisplaced. At 0 % eccentricity, the spike of transparent undisplaced fluid elongates back to over half of the test section. This is a clear indication of the effect of eccentricity.

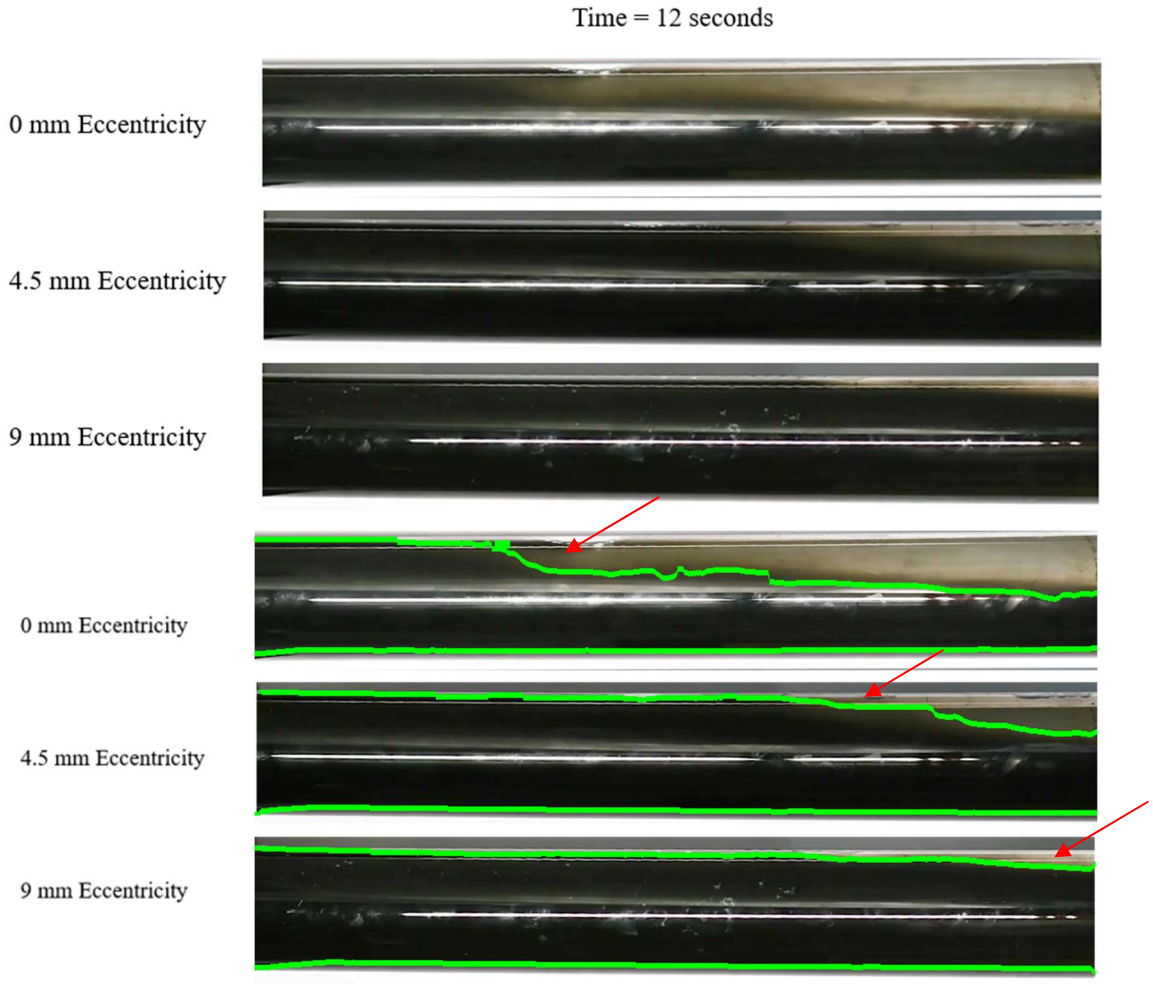

Figure 4.5 – Displacement fronts of 0 %, 46 % and 92 % eccentricity at time = 12 seconds. In addition, the computer image analyzed image is included to better help detect the interface of the fluids.

4.2.1 Summary of Results - Eccentricity

Figure 4.2- 4.5 show the significant effect eccentricity has on the system. Section 3.1.4 Gravity vs. Eccentricity describes the counteraction between the two forces. Eccentricity is said to promote flow on the upper wide part of the annuli. This is clearly illustrated in for instance, Figure 4.2, where the experiment with zero eccentricity (and hence is not affected by it) has a characteristic slumping displacement front. This means that the density difference, and therefore the gravitational force, is the dominant force in the system. In the experiment with 92 % eccentricity however, the effect of eccentricity increases, and a different

displacement front is observed. The front is still impacted by the density difference (gravity), but now the eccentricity is more dominant in the system. This switch of force dominance results in a more even and uniform displacement front. Consequently, a more steady piston like and ideal displacement is observed.

4.3 Effect of vibration

In this section the effect of vibration is studied. Test runs with different vibration intensities with the same eccentricity is compared. The results are presented as a series of images comparing the displacement fronts of the different runs. At each series of experiments, flow rate, densities, viscosities and eccentricity has been kept constant. Vibration is studied by increasing vibration intensity in three steps from low (2.48 Hz), medium (4.95 Hz), to high (10.73 Hz).

4.3.1 Series 1 – Concentric Annulus (0 % Eccentricity)

Table 4.1 Experimental parameters for Serie 1 – Concentric Annulus

series	Density, Displaced	Density, Displacing	Viscosity, Displaced	Viscosity Displacing	Flow rate	Vibration intensity	Eccentricity
1	998 kg/m^3	1111 kg/m^3	1 mPa*s	2.5 mPa*s	6 l/m	2.48 Hz, 4.95 Hz and 10.73 Hz	0 %

The annulus is concentric and not affected by eccentricity. Therefore, in this series, the counteraction between flow rate and gravity is studied and as well as how the vibration acts on the system. Even though it is not very likely to have a perfect concentric annulus in a horizontal well. It serves as a good reference or base line to the other test series and provides insight into the mechanisms of more optimal conditions.

Figure 4.6 displays the propagation of the black displacing fluid displacing the transparent fluid of Series 1 at time = 3 seconds. At this time, the displacement front of the run with zero vibration, is less advanced in the annulus compared to the runs influenced by vibration. Moreover, for the displacing front influenced by the highest vibration, the black displacement front is better distributed in the annulus and a more ideal front is observed. The front impacted by low- and medium vibration, seems however, not to be as well distributed as the high vibrations.

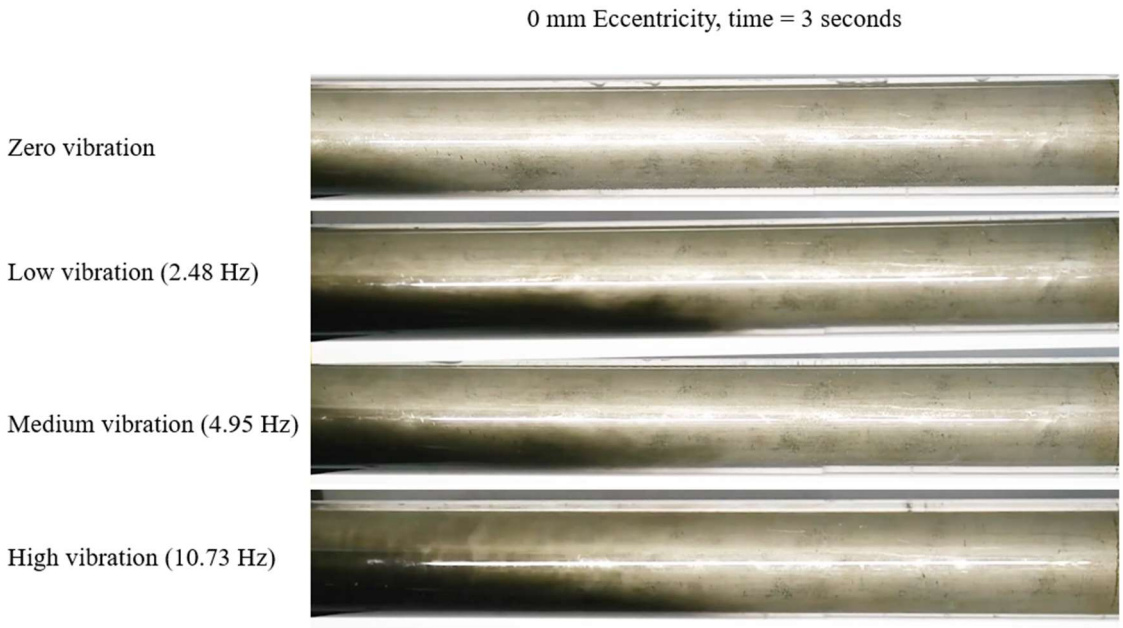

Figure 4.6 – Displacement fronts of Series 1 – Concentric Annuli at time =3 s with experimental runs: zero-, low- (2.48 Hz), medium- (4.95 Hz) and high vibration (10.73 Hz)

Figure 4.7 show the displacement fronts of the experimental runs of Series 1 at time = 6 seconds. At this time, the effect of high vibration becomes more apparent. The run without vibration is clearly stratified with a slumping front. Furthermore, the runs with low- and medium- vibration are rather similar to the run without vibration.

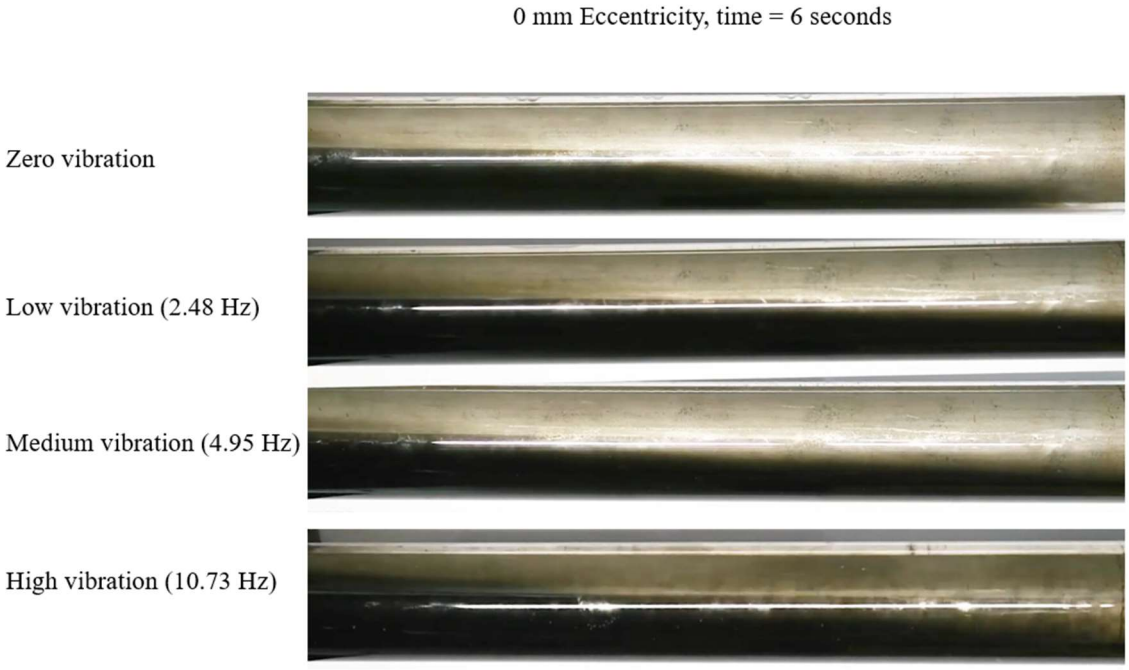

Figure 4.7 – Displacement fronts of Series 1 – Concentric Annuli at time = 6 s with experimental runs: zero-, low- (2.48 Hz), medium- (4.95 Hz) and high vibration (10.73 Hz)

Figure 4.8 displays the fronts of Series 1 at time =12 seconds. The figure show that the displacement influenced by high vibration is nearly completed, while the other three runs are not quite as advanced in the process. Interestingly, the test run without vibrations seems to be slightly further along in the process than for the two runs with low- and medium vibrations. This may indicate that the effect does not become prominent before reaching higher vibrations

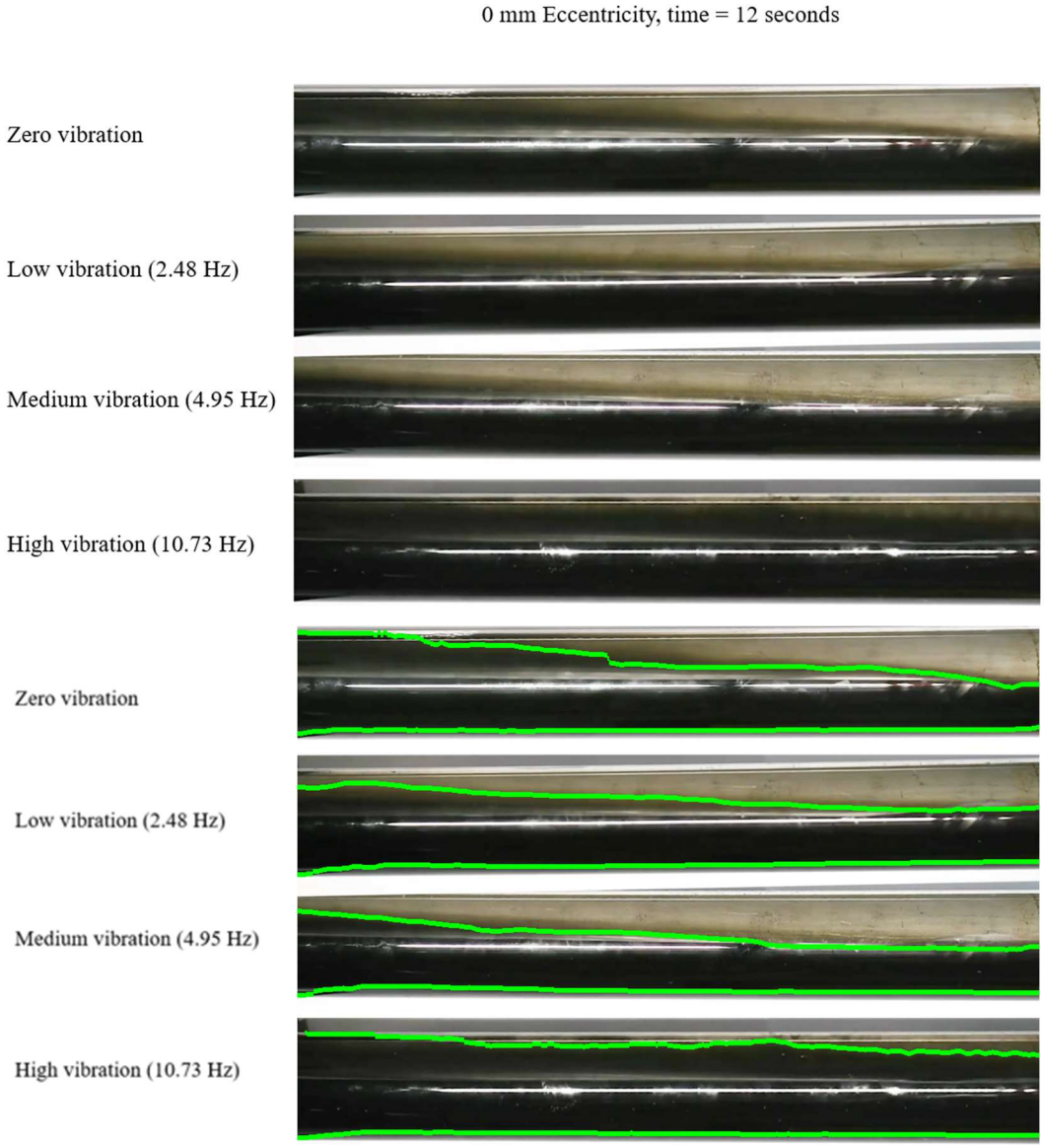

Figure 4.8 – Displacement fronts of Series 1 – Concentric Annuli at time = 12 s with experimental runs: zero-, low- (2.48 Hz), medium- (4.95 Hz) and high vibration (10.73 Hz). In addition, the computer image analyzed image is included to better help detect the interface of the fluids.

Figure 4.9 show the experimental runs of Series 1 at time = 15 seconds. Now, the high vibration run is completed while the run without vibration is nearly completed. A red arrow illustrates where some nondisplaced fluid is left in the annulus. The low- and medium-vibration, is however, not nearly finished. A long-elongated spike of nondisplaced transparent fluid can be observed. This may indicate that, the displacement process is not improved by the low- and medium vibration intensity.

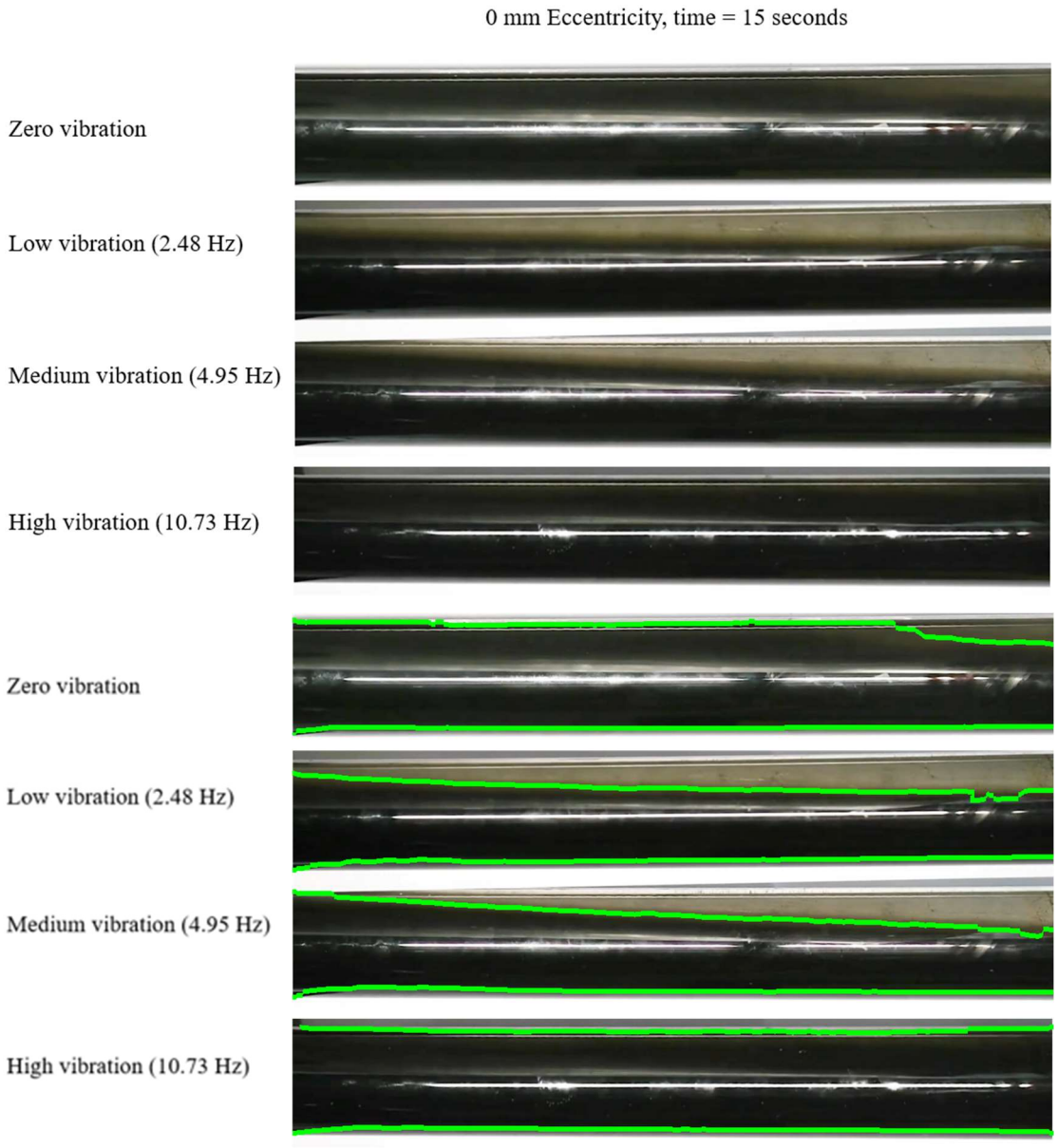

Figure 4.9 – Displacement fronts of Series 1 – Concentric Annuli at time = 15 s with experimental runs: zero-, low- (2.48 Hz), medium- (4.95 Hz) and high vibration (10.73 Hz). In addition, the computer image analyzed image is included to better help detect the interface of the fluids.

4.3.2 Serie 2 –Eccentric Annulus (46 % Eccentricity)

Table 4.2 Experimental parameters for Serie 2 – Eccentric Annulus

series	Density, Displaced	Density, Displacing	Viscosity, Displaced	Viscosity Displacing	Flow rate	Vibration intensity	Eccentricity ->
2	998 kg/m^3	1111 kg/m^3	1 mPa*s	2.5 mPa*s	6 l/m	2.48 Hz, 4.95 Hz and 10.73 Hz	46%

In Serie 2 the annulus is set to an eccentric position, which is a very likely position for the annulus in a horizontal well.

Figure 4.10 illustrates the displacement fronts of the experimental runs of Serie 2 at time = 3 seconds. In general, all the displacement fronts of the runs at this time is seen to be rather even and well distributed. Nevertheless, one can argue that the front of the medium vibration run seems to be somewhat less optimal compared to the others.

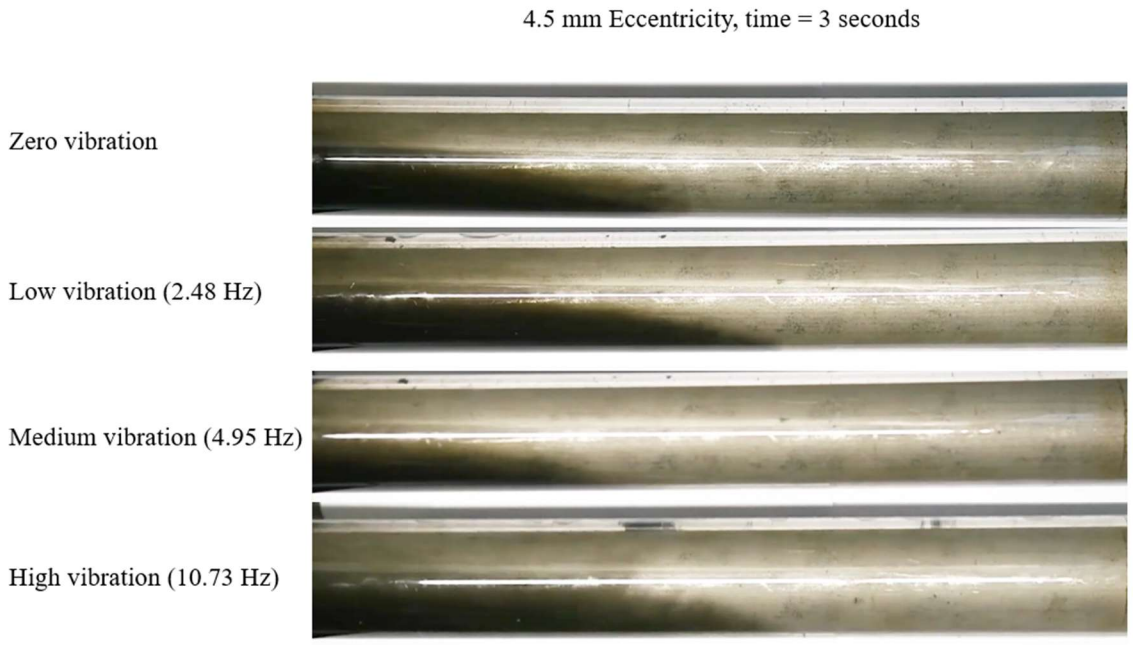

Figure 4.10 – Displacement fronts of Series 2 – Eccentric Annuli at time = 3 s with experimental runs: zero-, low- (2.48 Hz), medium- (4.95 Hz) and high vibration (10.73 Hz)

Figure 4.11 illustrates the displacement fronts of the experimental runs of Serie 2 at time = 6 seconds. At this time, the effect of high vibration seems to be more evident. The run with high vibration has an elongated spike at the top of the annulus, but the black transparent fluid dominates the annulus more in this run, in contrast to the other runs.

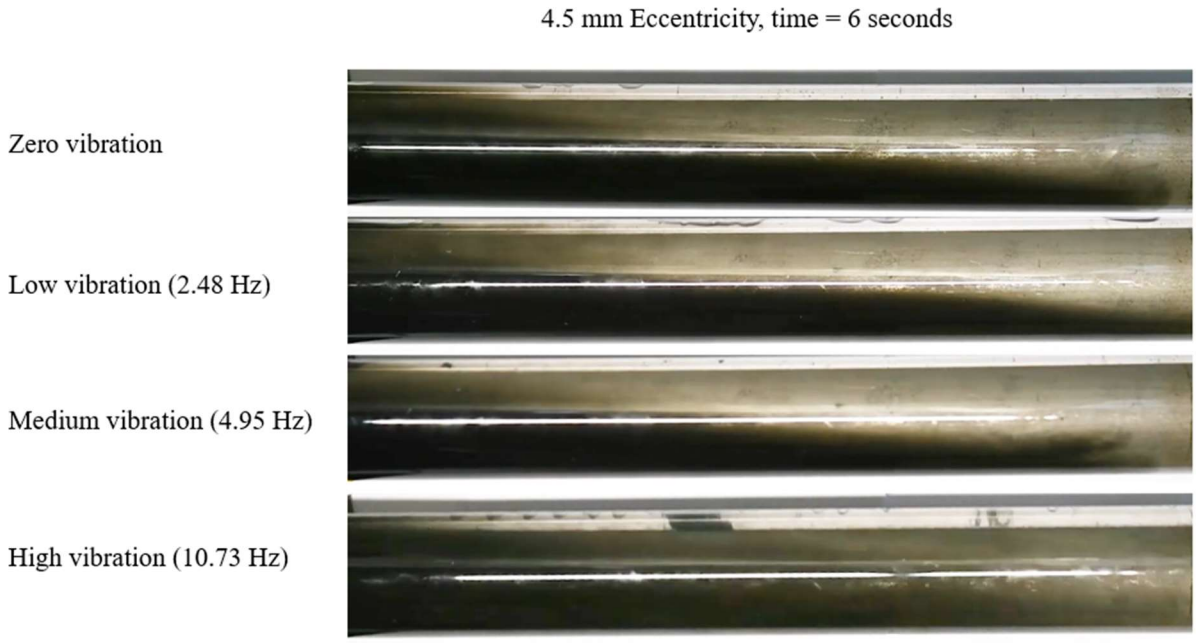

Figure 4.11 – Displacement fronts of Series 2 – Eccentric Annuli at time = 6 s with experimental runs: zero-, low- (2.48 Hz), medium- (4.95 Hz) and high vibration (10.73 Hz)

Figure 4.12 shows the displacement fronts of the experimental runs of Serie 2 at time = 12 seconds. The red arrows illustrate where the end of the elongated undisplaced spike is positioned. At this time, the high vibration run is nearly finished. The zero- low- and medium vibration runs has a somewhat extended elongated spike, where the medium vibration run appear to be the least advanced of them all.

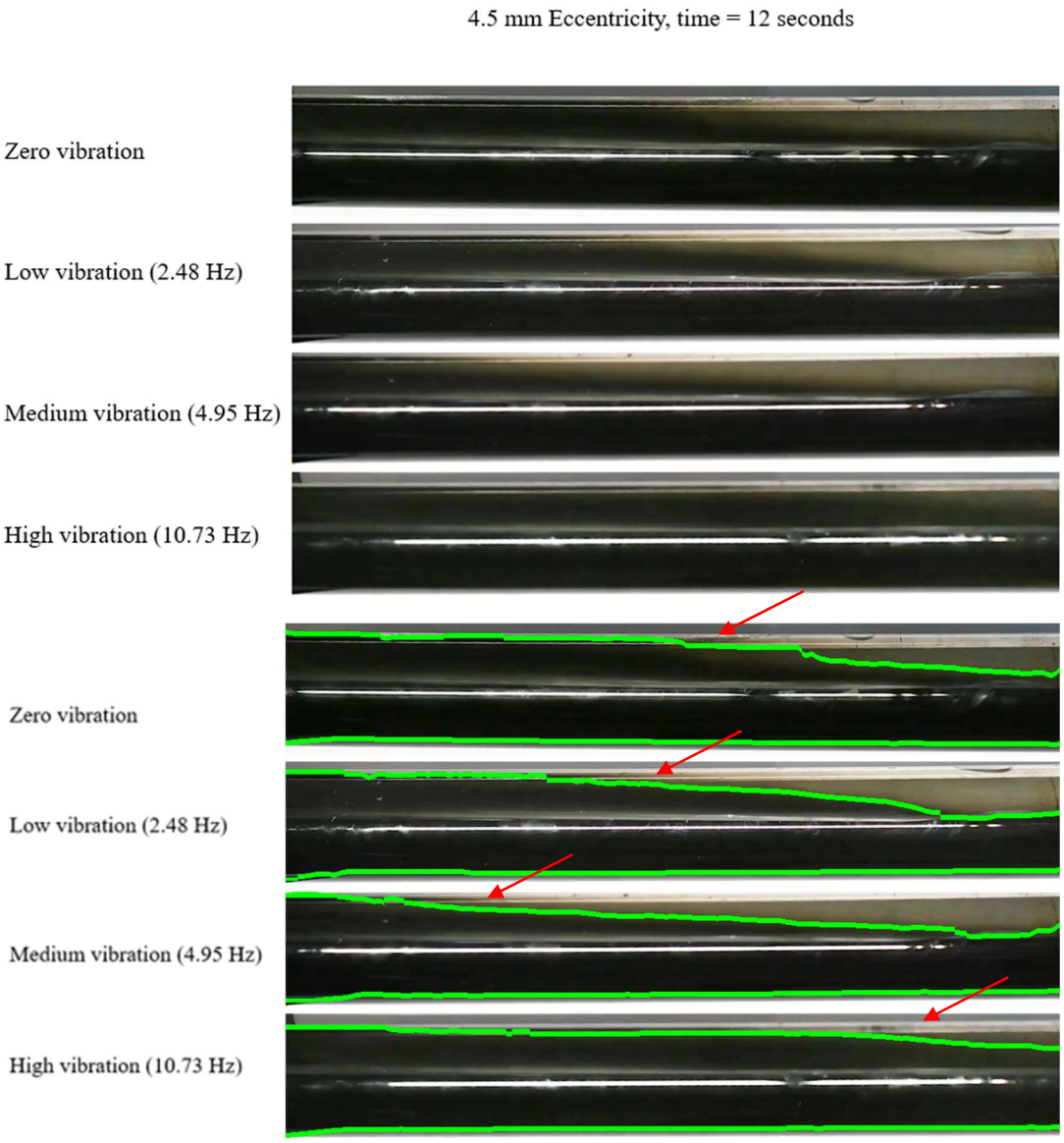

Figure 4.12 – Displacement fronts of Series 2 – Eccentric Annuli at time = 12 s with experimental runs: zero-, low- (2.48 Hz), medium- (4.95 Hz) and high vibration (10.73 Hz). In addition, the computer image analyzed image is included to better help detect the interface of the fluids.

Figure 4.13 illustrates the displacement fronts of the experimental runs of Serie 2 at time = 15 seconds. Now, both zero- and high vibration is completed, whereas the low- and middle vibration seem to be relatively similar positioned in their displacement process.

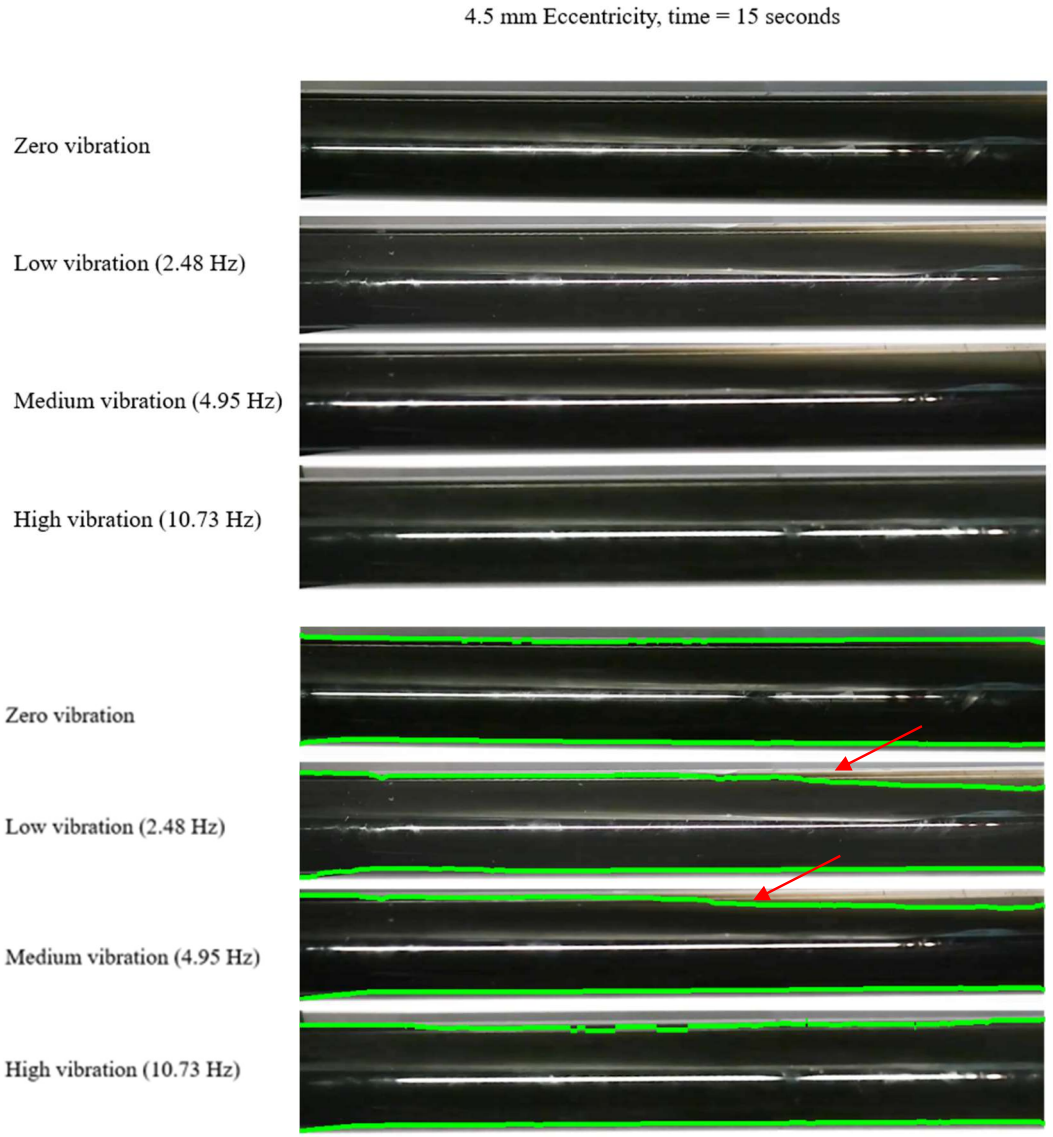

Figure 4.13 – Displacement fronts of Series 2 – Eccentric Annuli at time = 15 s with experimental runs: zero-, low- (2.48 Hz), medium- (4.95 Hz) and high vibration (10.73 Hz). In addition, the computer image analyzed image is included to better help detect the interface of the fluids.

4.3.3 Serie 3 – Strongly Eccentric Annulus (92 % Eccentricity)

Table 4.3 Experimental parameters for Serie 3 – Strongly Eccentric Annulus

series	Density, Displaced	Density, Displacing	Viscosity, Displaced	Viscosity Displacing	Flow rate	Vibration intensity	Eccentricity ->
3	998 kg/m^3	1111 kg/m^3	1 mPa*s	2.5 mPa*s	6 l/m	2.48 Hz, 4.95 Hz and 10.73 Hz	92%

In Serie 3 the annulus is set to a strongly eccentric position, a position which may be likely for the annulus in some areas in a horizontal well.

Figure 4.14 displays the displacement fronts of the experimental runs of Serie 3 at time = 3 seconds. In this Series, an interesting shift is observed; the three displacements, zero-, low- and medium vibration, all tend to flow along the middle to lower part of the annulus. the high vibration run is primarily displaced in the upper wide part of the annulus. Nevertheless, all four is fairly well distributed.

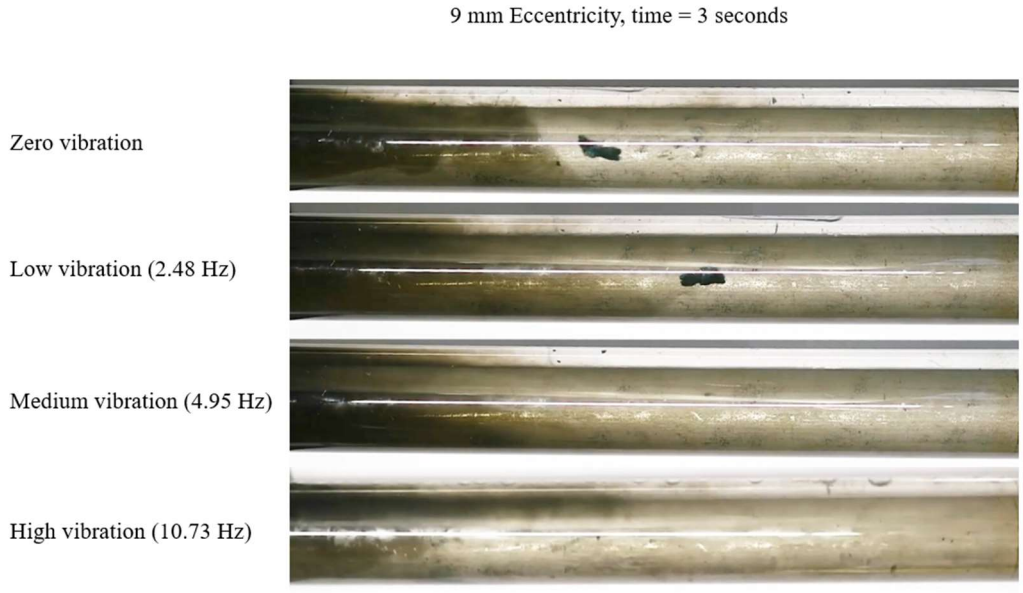

Figure 4.14 – Displacement fronts of Series 3 –Strongly Eccentric Annuli at time = 3 s with experimental runs: zero-, low- (2.48 Hz), medium- (4.95 Hz) and high vibration (10.73 Hz).

Figure 4.15 show the displacement fronts of the experimental runs of Serie 3 at time = 6 seconds. At this time, the effect of eccentricity and vibration in combination is furthered visualized and clearly demonstrated.

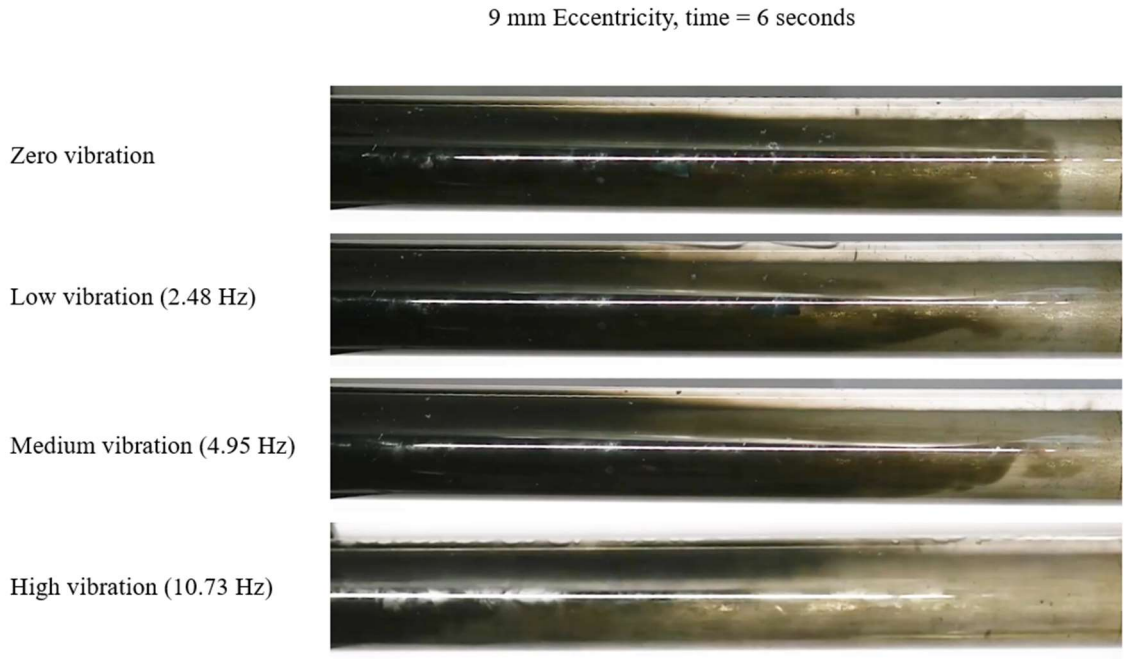

Figure 4.15 – Displacement fronts of Series 3 –Strongly Eccentric Annuli at time = 6 s with experimental runs: zero-, low- (2.48 Hz), medium- (4.95 Hz) and high vibration (10.73 Hz)

Figure 4.16 show the displacement fronts of the experimental runs of Serie 3 at time = 12 seconds. At this time, all the displacements are nearly completed, and the red arrows indicate the starting point of the elongated undisplaced spike of transparent fluid. Once again, the shift of the elongated spike is seen in the high vibration run.

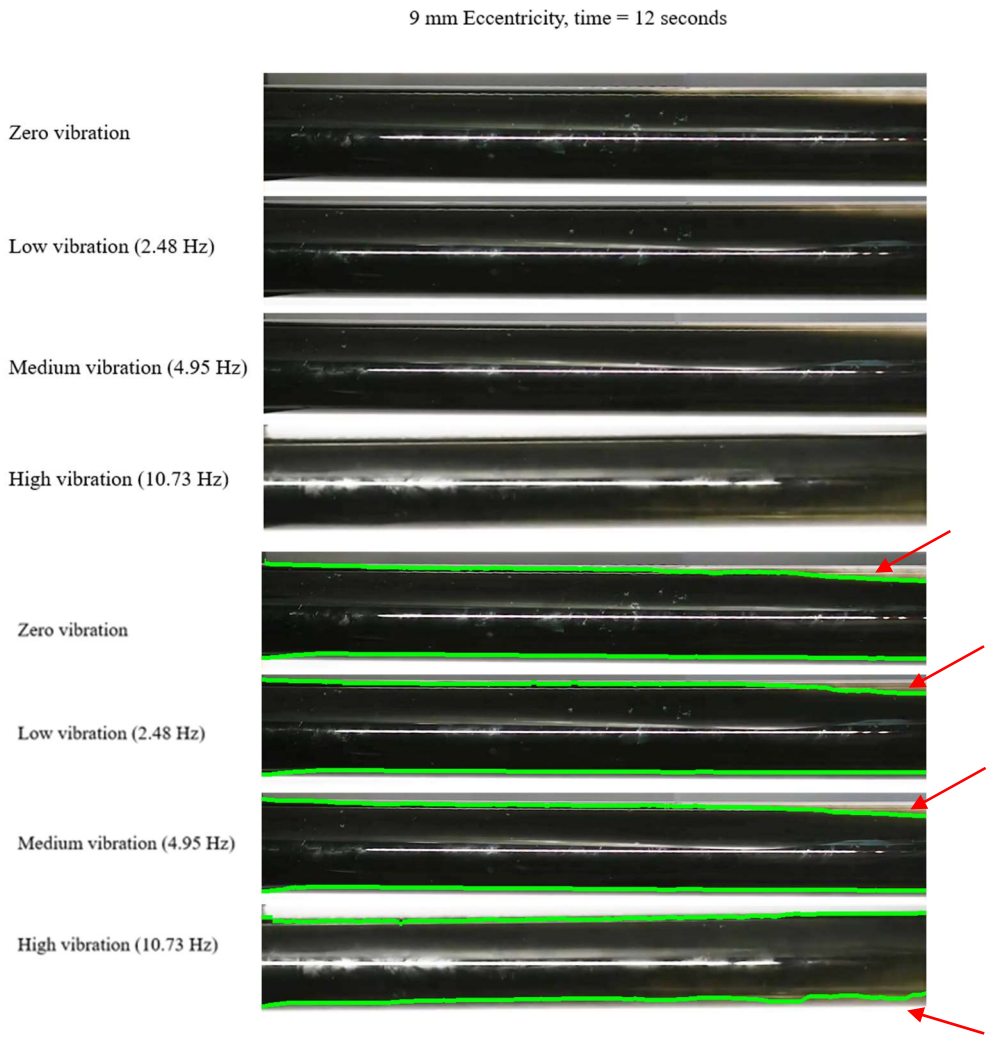

Figure 4.16 – Displacement fronts of Series 3 –Strongly Eccentric Annuli at time = 12 s with experimental runs: zero-, low- (2.48 Hz), medium- (4.95 Hz) and high vibration (10.73 Hz). In addition, the computer image analyzed image is included to better help detect the interface of the fluids.

4.3.4 Summary of Results - Vibration

Figure 4.6 – 4.16 provides a good base for the analysis of the effect of vibration. As shown in the various experiments, the counteraction is between gravity and flow rate with eccentricity. Consequently, gravity will promote flow on the lower side, while flow rate and eccentricity promotes flow on the upper side. In addition, vibration will act on the system. It promotes fluid flow on both the upper and lower part of the annulus by 'pushing' black displacing fluid up and down. The impact of vibration is seen throughout Series 1-3. It is well illustrated when comparing the 46 % and 92 % eccentricity runs, both with high vibrations. In the 46

% eccentricity high vibration run, vibrations contributes to push the black displacing fluid onto the upper part, assisting in a more even and ideal displacement by counteracting the force of gravity (Figure 4.11). In the 92 % eccentricity high vibration run, the vibration assists in promoting flow onto the lower part of the annulus and by this, balancing out the force of eccentricity and flow rate, (Figure 4.15). These experiments provide a good indication that high vibration will improve the displacement process by promoting flow of the black displacement fluid in the undisplaced area, either in the upper or lower part of the annulus.

Though the high vibration appear to have a beneficial impact on the system, the effect does not seem to be to be particularly advantageous for low- and medium vibration. It appears that there is some kind of threshold for how much vibration is needed before observing a positive effect. The vibrations, particularly the lower vibrations, seems not to have the same ability to create the desired orbitational flows compared to rotation. The vibration tend to have a lateral and axial movement rather than a rotational movement. Consequently, a higher vibration intensity is needed to obtain a satisfactory result.

4.4 Uncertainties

When performing the laboratory experiments, some uncertainties were unavoidable. In some of the experiments, there was an issue of air bubbles in the test section. The hoses from the reservoir tanks to the annulus and pulse dampener, were placed as high above the ground as possible, trying to prevent air bubbles to flow into the annulus, but still it was not possible to completely avoid bubbles. Unfortunately, this may have affected the displacement front somewhat. As the bubbles has a higher velocity than the liquids, they will impose a higher velocity on the displacement front resulting the front affected by air bubbles to be displaced quicker. For this reason, some test runs were performed repeatedly, but for runs influenced by high vibration and strong eccentricity, it was simply not possible to avoid for some of them. However, these air bubbles were taken into account when performing the result analysis and did not affect the final results.

The available flow meter did not perform properly and could not be used. Therefore, the flow velocity was measured manually (see section 4.5 Flow Meter for a description of the process). Although the flow rate was measured multiple times, one cannot exclude the possibility of some minor offset from its desired velocity of 6 l/min. However, the flow rate was set at a fixed speed and not adjusted further, thus all the experimental runs was subjected to the same

flow velocity. Besides, a small error in the flow velocity would not significantly affect the results, nor the dimensionless parameters such as Froude- and Reynolds number.

4.5 Discussion

The main objectives for this study was to investigate whether there under any conditions would exist a steadier displacement by studying how varying the vibrations frequency and eccentricity affect annular displacement.

In the sections below, these conditions have been discussed by comparing the different eccentricities and vibrations, - comparing them to the theory and previous research as laid out in chapter 2, and to the objectives as laid out above.

4.5.1 Eccentricity

The findings in this study clearly indicates that eccentricity will promote fluid to flow on the upper wide part of the annulus in a horizontal section. It also shows with regards to the counteractions between eccentricity with flow rate and gravity, that if eccentricity becomes sufficiently strong, it will balance out the force of gravity, which will result in a more even and uniform displacement.

Furthermore, in Chapter 3.1 Displacement in the Annulus, the negative effects eccentricity has on the displacement process is stated. However, in the presented results in Section 4.1 Effect of Eccentricity, the displacement profile seems to be improved by eccentricity. Superficially, the theory and results appear to be in conflict. Although eccentricity does restrict flow on the constricted side of the annulus, there is almost no friction nor pressure difference between the constricted and less constricted side present in the laboratory test experiments. Another factor is that the flow rate of fluids are relatively low. This is important parameters which influence fluid to flow on the less constricted part. It should be noted that in a real cementing operation and also hence in theory all parameters regarding a cementing and displacement process is considered. Challenges such as particle sedimentation, high yield and gel strengths are intensified by the increase of eccentricity. Consequently, eccentricity contributes to a more challenging displacement process (Nelson & Guillot, 2006).

The findings in this study coincides well with existing research on the topic. In Chapter 3.5 Previous Research, Section 3.5.1 General overview, a selection of earlier studies were presented. In these research investigations, all studies concluded that eccentricity does drive fluid to flow over to the less constricted side of the annulus. In addition, there were great consensus that mobilizing fluid in the constricted side of the annulus is key to a good displacement process.

Moreover, in Chapter 3.5 Previous research, Section 3.5.2 Horizontal Eccentric Annuli, the work of Carrasco-Teja (2008) and Renteria & Frigaard (2020) was presented. The studies both investigated the underlaying counteraction between eccentricity and gravity (buoyancy) by CDF simulations and laboratory experiments. Renteria & Frigaard (2020) described how the displacement flow would either have a slumping- or 'top side' front, depending on whether respectively, eccentricity and flow rate or gravity (buoyancy) would be the dominating the system. This description of displacement fronts concurs well with the results in this study where the slumping displacement front was the dominating front found in the experiments.

4.5.2 Vibration

The findings in this study indicates for test runs subjected to the highest vibration intensity (8 Hz), a more even and steady displacement was found. The high vibration intensities will promote fluid flow in the entire area of the annulus; both on the wide and narrow part. This results in an improved displacement process. However, regarding low- and medium vibration, the displacement process did not show a significant improvement when influenced by low- and medium vibration. The reason for this is thought to have something to do with the vibrational movements. The vibration tool used in this study generated mostly axial-and lateral- rather than rotational vibrations.

Chapter 2.5 Effect of Pipe Movement describes how rotation can generate an orbitational flow called Taylor vortices. This flow is particularly beneficial for promoting fluid to be mobilized throughout the entire annular area, even when influenced by gravity. From the results in Section 4.2 Effect of vibration, it seems that axial and lateral vibration does not have the

ability to create orbitational flows. Thus, to mobilize fluid flow in the entire annular area a high vibration intensity is required.

The results of the experiments may indicate that a displacement process without vibration is favored compared to the process with low- and medium vibrations which is contradicting common theories and field observations. This was described and discussed in Section 4.2 Effect of Eccentricity, where laboratory limitations such as pipe friction and pressure differences were described. In the same chapter it was discussed that it was not possible to recreate field experience with regards to cementing challenges like particle sedimentation and high yield/ gel strength in the lab model. And as stated in the book 'Well Cementing', such type of challenges may be somewhat less aggravated when utilizing vibration (Nelson & Guillot, 2006). The results also reflects that the experiments are performed under optimized conditions, and the actual beneficial impact of vibration becomes less clear. Evidently, the displacement process without vibration may seem preferable, even though, this is not necessarily the case in a real cementing operation.

In Chapter 2.6 Previous research section 2.5.3 Casing/ Tubing Rotation- and Vibration Research a selection of earlier studies were presented. Thom et. al. in association with Shell UK Ltd (2016) investigated the possibility of using a vibration tool for a subsea P&A operation. They found that vibration was an advantageous tool for decreasing undesirable high gel strengths in old drilling fluid. This is an important addition to the study of vibration tools. However, this study was performing experiments with Newtonian fluids, and thus, did not have the ability to investigate gel strength decay as a result of vibration. Moreover, the experiments was performed under optimized conditions. Therefore, the actual beneficial impact of vibration becomes less clear. For this reason, the displacement process without vibration may seem preferable, even though, this is not necessarily the case in a real cementing operation.

4.5.3 Conductivity measurement

To study the displacement front, conductivity measurements was performed throughout the experiments. When processing the data, it became evident that the results were inconclusive. The root cause investigation pointed at several factors: - the test rig being in a horizontal position, - both inlet and outlet in the bottom of the pipe, - conductivity meter mounted downstream of the outlet (Figure 4.17), - gravitation force. This resulted in mixing of the clear

and black displacements fluids at the reading point of the meter, even though the fluids had been separated in the test pipe. As a consequence, the conductivity meter transmitted readings with graphs that was not comparable between the different experiments. The conductivity data can be found in Appendix A.

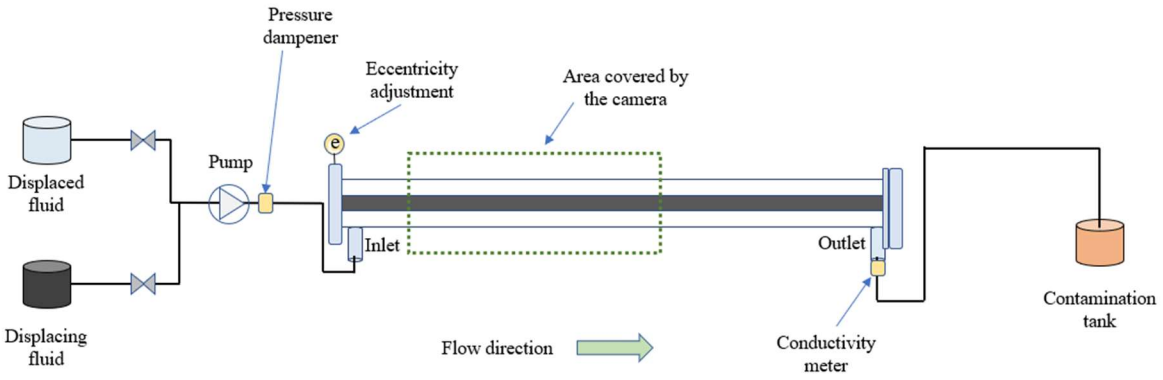

Figure 4.17 – Schematic of the horizontal rig test set up.

5 Conclusion

Displacement efficiency experiments were conducted on a horizontal test rig to study how varying the vibration intensity and eccentricity would affect annular displacements. The task was also to investigate whether there under any conditions would exist a steadier displacement.

To study the isolated effect of eccentricity on a horizontal displacement profile, flow rate, densities and viscosities were kept constant while vibration was set to zero. Throughout all the experimental runs, the counteraction of eccentricity between flow rate and gravity was clearly observed. Eccentricity promoted fluid to flow on the upper wide part of the annulus while gravity (density difference) promoted fluid to flow on the lower part of the annulus. The results of the experimental tests showed that gravity was the dominating force in the system, consequently resulting in a slumping displacement front. Nevertheless, as eccentricity increased, the gravitational force became less dominating and a more even and steady piston like displacement front was observed. The findings in this study coincides well with existing research on the topic described in Section something.

The effect of vibration was investigated by comparing different vibration intensities with adjustment of eccentricities. For these experimental runs, vibration mainly acted on the system, with the counteraction between gravity, flow rate and eccentricity still present. Vibration promoted fluid to flow in the entire area of the annulus; both on the upper wide part and the lower narrow part. The black displacement fluid was pushed laterally and axially in the annulus, resulting in a more evenly distributed and steadier displacement front. The high vibration intensity seemed to be especially advantageous for increasing the displacement efficiency. However, the low- and medium- vibrations did not appear to significantly improve the displacement efficiency. There seems to be a certain threshold for how much vibration is needed for a positive effect to be observed. This is thought to be connected with the vibrational movement. The vibration tool used in this thesis generally generates lateral and axial movement rather than rotational movement. Moreover, these lateral and axial movement does not appear to have the same ability in creating desired orbitational flows compared to rotation. Consequently, a high vibration intensity is needed to obtain a satisfactory result.

5.1 Recommendations for Further Work

This thesis contributes to bridging the knowledge gap of the vibration-assisted cementing research, where it was found that high vibration intensities does seem to improve the displacement efficiency. Nevertheless, further investigations are still needed to highlight areas of interest. In addition, a summary of improvements areas of the experimental set-up is given.

Due to the COVID-19 pandemic, the allocated laboratory time period was unfortunatly shortened. Therefore, the main focus in this thesis has been the effect of using a vibration tool at various speeds and eccentricity on Newtonian fluids with relatively low viscosity and density while keeping all parameters such as densities, viscosities and flow rates constant.

It is recommended to study how the vibration tool would act on a system with non-Newtonian fluids with higher viscosities. This could provide more insight in how the vibration tool could decrease high undesirable gel- and yield stregths.

This thesis studied horizontal displacement profiles, a recomandation would be to perform similar tests on an inclined test set up to study the effect on vibration. Furthermore, installing control lines to examine how this would influence the displacement.

To investigate the effect of flow velocity on the displacement efficiency varying the flow rate could provide more insight into the underlaying counteraction of forces between eccentricity with flow rate and gravity (density difference), further laboratory experiments is recommended.

The vibration tool used in this thesis generates mostly axial and lateral movement in the annulus in favor of rotational movement. To investigate how rotation will improve displacement using the vibration tool it would be recommended to study what effect this will have on the system.

For the experimental set up and visualization of the experiments, the following improvements are proposed:

- Installing a fish tank containing glycerol surrounding the test section with the purpose of optimize optical visualization to minimize reflections.
- A mirror on the backside of the test section to create a 360 degree view of the displacement process.
- To mimimize the air bubbles in the experiments, shorten the hoses from the fluid tanks to the test section.

References

Bolster, D., Hershberger, R., & Donnelly, R. (2011). Dynamic similarity, the dimensionless science. *Physics Today, 64*(9). doi:10.1063/PT.3.1258

Bu, Y., Tian, L., Li, Z., Zhang, R., Wang, C., & Yang, X. (2018). Effect of casing rotation on displacement efficiency of cement slurry in highly deviated wells. *Journal of Natural Gas Science and Engineering, 52*, 317-324. doi:https://doi.org/10.1016/j.jngse.2018.01.040

Caenn, R., Darley, H. C. H., & Gray, G. R. (2016). Introduction to Drilling Fluids. In *Composition and Properties of Drilling and Completion Fluids* (pp. 1-34): Oxford: Elsevier Science & Technology.

Carrasco-Teja, M., Frigaard, I. A., Seymour, B. R., & Storey, S. (2008). Viscoplastic fluid displacements in horizontal narrow eccentric annuli: stratification and travelling wave solutions. *Journal of Fluid Mechanics, 605*, 293-327. doi:10.1017/S0022112008001535

Çengel, Y. A., Cimbala, J. M., & Turner, R. H. (2017). Introduction to Fluid Mechanics. In *Fundamentals of thermal-fluid sciences* (Fifth edition]. ed., pp. 464-481). New York, N. Y.: McGraw-Hill Education.

Couturier, M., Guillot, D., Hendriks, H., & Callet, F. (1990). *Design Rules And Associated Spacer Properties For Optimal Mud Removal In Eccentric Annuli.* Paper presented at the Annual Technical Meeting.

Enayatpour, S., & van Oort, E. (2017). *Advanced Modeling of Cement Displacement Complexities.* Paper presented at the SPE/IADC Drilling Conference and Exhibition.

Haut, R. C., & Crook, R. J. (1979). *Primary Cementing: The Mud Displacement Process.* Paper presented at the SPE Annual Technical Conference and Exhibition.

Jakobsen, J., Sterri, N., Saasen, A., Aas, B., Kjosnes, I., & Vigen, A. (1991). *Displacements in Eccentric Annuli During Primary Cementing in Deviated Wells.* Paper presented at the SPE Production Operations Symposium.

JUMO. (2021). JUMO CTI-500 - Inductive Conductivity/Concentration and Temperature Transmitter with Switching Contacts (202755). Retrieved from http://www.jumo.net/products/as-per-approvals/metrological-certification/202755/jumo-cti-500---inductive-conductivity-concentration-and-temperature-transmitter-with-switching-contacts-202755.html

Keller, S. R., Crook, R. J., Haut, R. C., & Kulakofaky, D. S. (1987). Deviated-Wellbore Cementing: Part 1 - Problems. *Journal of Petroleum Technology, 39*(08), 955-960. doi:10.2118/11979-pa

Khalifeh, M., & Saasen, A. (2020a). Fundamentals of Plug Placement. In *Introduction to Permanent Plug and Abandonment of Wells* (pp. 185-212). Cham: Springer International Publishing.

Khalifeh, M., & Saasen, A. (2020b). *Introduction to Permanent Plug and Abandonment of Wells*(1st ed. 2020. ed., Vol. 12).

Lavrov, A., & Torsæter, M. (2016a). Fluid Flow and Displacement in the Annulus. In *Physics and Mechanics of Primary Well Cementing* (pp. 25-62). Cham: Springer International Publishing.

Lavrov, A., & Torsæter, M. (2016b). Properties of Well Cement. In *Physics and Mechanics of Primary Well Cementing* (pp. 9-23). Cham: Springer International Publishing.

Ma, K.-T., Luo, Y., Thomas Kwan, C.-T., & Wu, Y. (2019). *Mooring System Engineering for Offshore Structures*. San Diego: San Diego: Elsevier Science & Technology.

Malekmohammadi, S., Carrasco-Teja, M., Storey, S., Frigaard, I. A., & Martinez, D. M. (2010). An experimental study of laminar displacement flows in narrow vertical eccentric annuli. *Journal of Fluid Mechanics, 649*, 371-398. doi:10.1017/S0022112009993508

Nelson, E. B., & Guillot, D. (2006). *Well cementing* (2nd ed. ed.). Sugar Land, Tex: Schlumberger.

NORSOK Standard D-010. (2021). In *Well integrity in drilling and well operations. Standards Norway*. Standards Norway.

Rapp, B. E. (2017). *Microfluidics : modeling mechanics and mathematics*(First edition. ed.).

Rehm, B., & International Association of Drilling, C. (2008). *Managed pressure drilling*. Houston, Tex: Gulf Publ. Co.

Renteria, A., & Frigaard, I. A. (2020). Primary cementing of horizontal wells. Displacement flows in eccentric horizontal annuli. Part 1. Experiments. *Journal of Fluid Mechanics, 905*, A7. doi:10.1017/jfm.2020.713

Schlumberger. (Ed.) (2021) Oilfield Glossary. Schlumberger.
Skadsem, H. J., Kragset, S., & Sørbø, J. (2019). *Cementing an Irregular Annulus Geometry: Full-Scale Experiments and 3D Simulations.* Paper presented at the SPE/IADC International Drilling Conference and Exhibition.
Tehrani, A., Ferguson, J., & Bittleston, S. H. (1992). *Laminar Displacement in Annuli: A Combined Experimental and Theoretical Study.* Paper presented at the SPE Annual Technical Conference and Exhibition.
Thom, F., Angell, P., Greig, N., Robertson, N., & Hogg, H. (2020). *Case Study for Rig-Less Subsea Well Abandonment.* Paper presented at the SPE/ICoTA Well Intervention Conference and Exhibition.
Verder-Liquids. (2021). Verderflex Rollit Peristaltic Hose Pumps. Retrieved from https://www.verderliquids.com/fileadmin/user_upload/Website_documents_2016/Verderflex/Documents/Documents_EN/Rollit/Rollit_25_P_Techno_Metric.pdf
Youngs, D. L. (1991). Three-dimensional simulation of the mixing of miscible fluids by Rayleigh–Taylor instability. *Physics of Fluids A : Fluid Dynamics, 3*(5), 1312-1320. doi:10.1063/1.858059
Aadnøy, B. S., & Society of Petroleum, E. (2009). *Advanced drilling and well technology*. Richardson, Tex: Society of Petroleum Engineers.
Aas, B., Sørbø, J., Stokka, S., Saasen, A., Statoil, R. G., Lunde, Ø., . . . Vrålstad, T. (2016). *Cement Placement with Tubing Left in Hole during Plug and Abandonment Operations.* Paper presented at the IADC/SPE Drilling Conference and Exhibition.

Appendix A

A.1 Conductivity Measurements

The results of the conductivity measurements were inconclusive and thus not considered in the results and discussion of the thesis. Nevertheless, the readings of the conductivity meter is can be found in Figure A.1

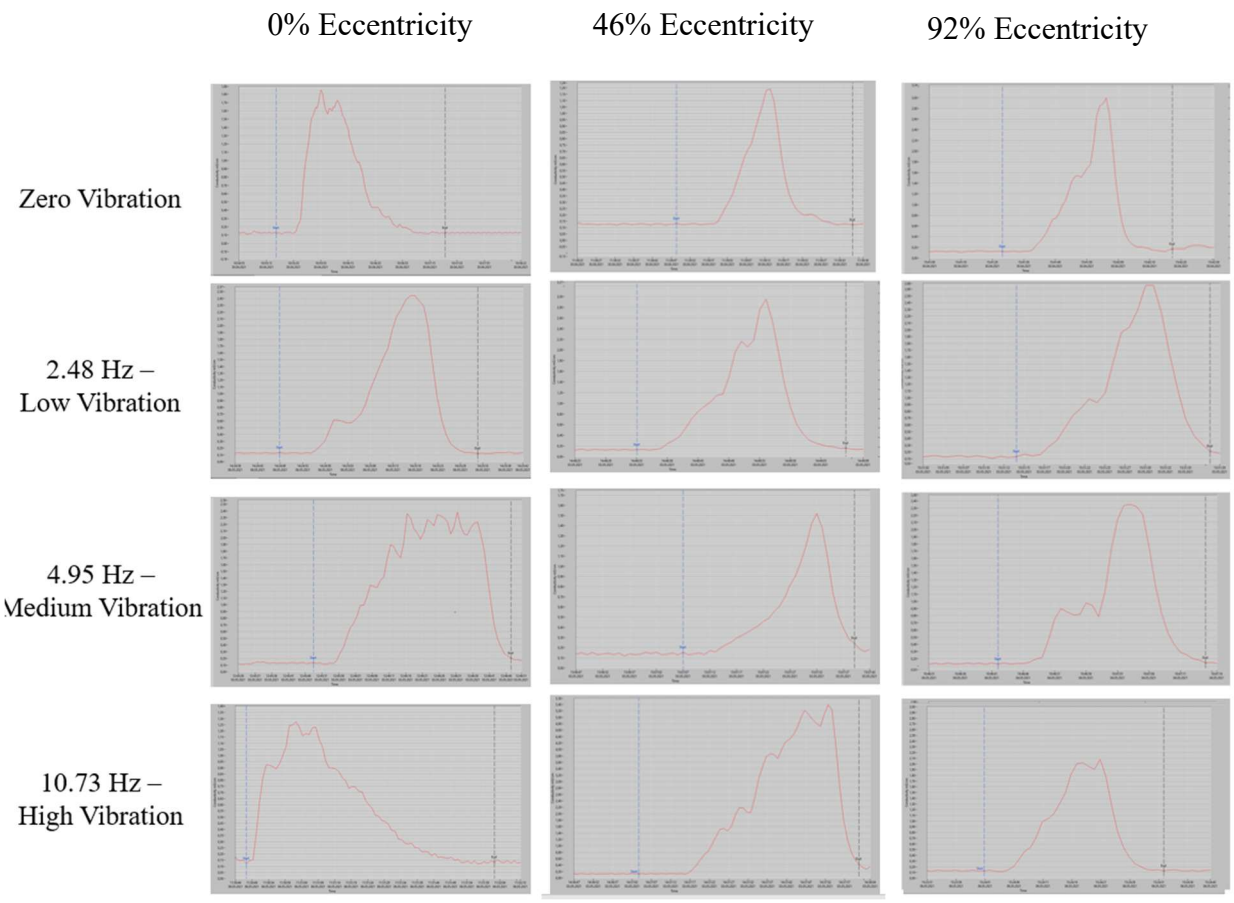

Figure A.1 – conductivity measurements of 0%, 46 % and 92% eccentricity with zero, low, medium and high vibrations

A.2 Conductivity Calibration

A conductivity meter is calibrated by inserting the conductivity probe into three different saline water solutions containing different percentages of salt. To investigate whether the conductivity meter is calibrated correctly, the transmitted conductivity readings is plotted with the salt percentage. If there is a linear relating between conductivity readings and salt percentage, the conductivity meter is calibrated correctly. For the purpose of this experiments, the saline water solutions contained 1%, 3% and 5% of salt, this resulted in conductivity measurements listed in Table A.1. Figure A.2 shows the linear relationship of conductivity measurements and salt percentage; thus, the conductivity meter was calibrated correctly.

Table A.1 Result of Conductivity Calibration

Conductivity Measurement	Salt concentration
19	1%
48	3%
76	5%

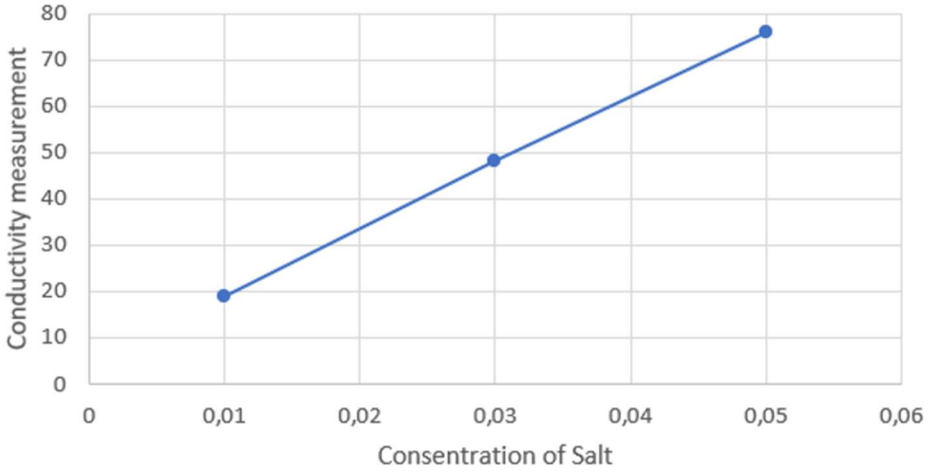

Figure A.2 – the plotted relationship of conductivity measurements and concentration of salt

Appendix B

1 Computer Image Analysis

A computer image analysis program was created to locate the interface of the displacing and displaced fluid. The produced images of this analysis program can be found below.

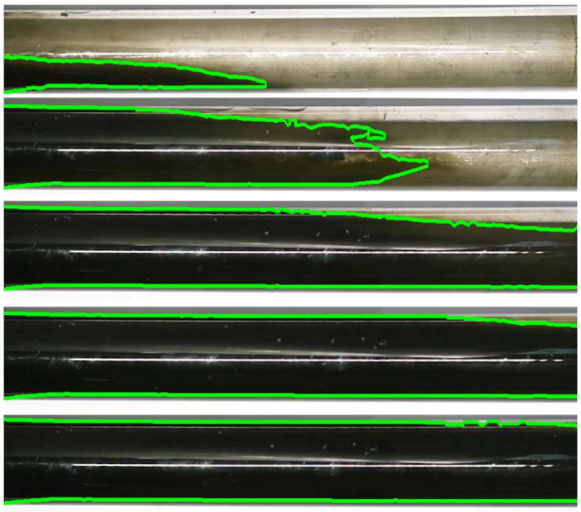

Figure B.1 – Image analysis of Figure 4.1

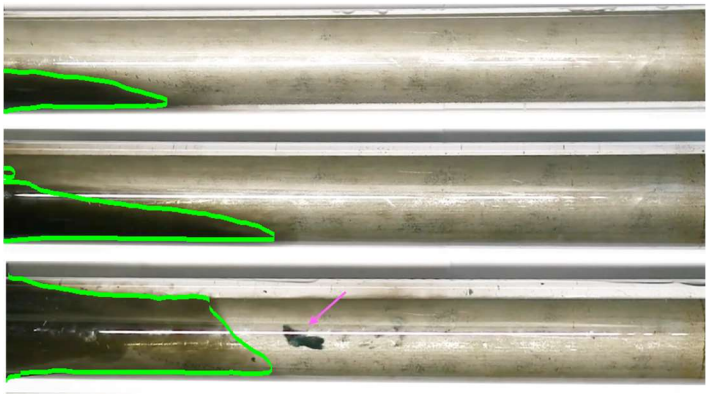

Figure B.2 – Image analysis of Figure 4.3

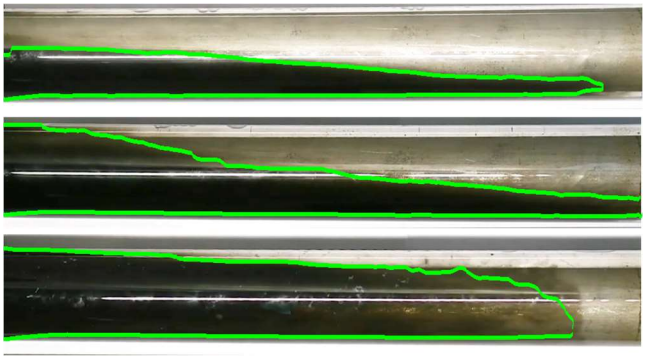

Figure B.3 – Image analysis of Figure 4.4

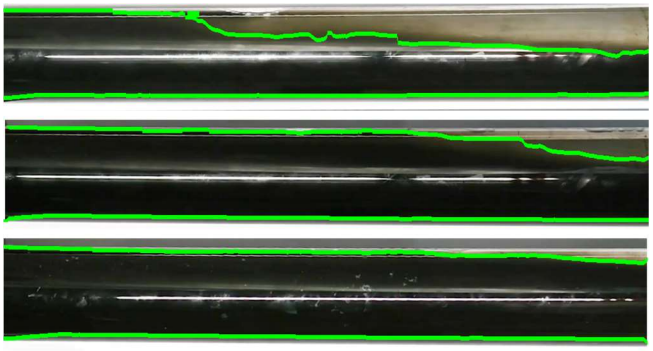

Figure B.4 – Image analysis of Figure 4.5

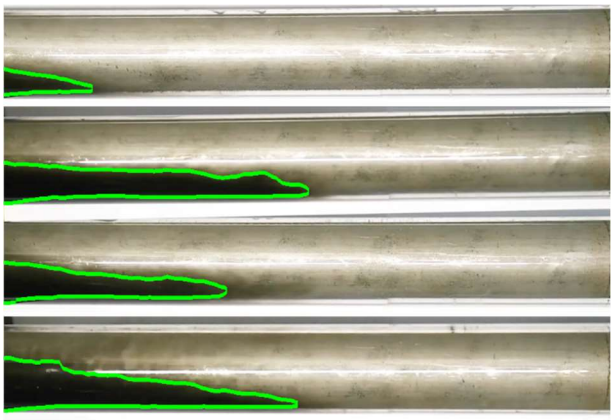

Figure B.5 – Image analysis of Figure 4.6

Figure B.6 – Image analysis of Figure 4.7

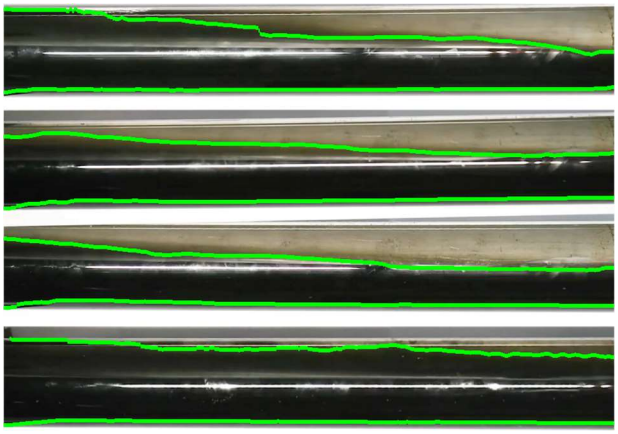

Figure B.7 – Image analysis of Figure 4.8

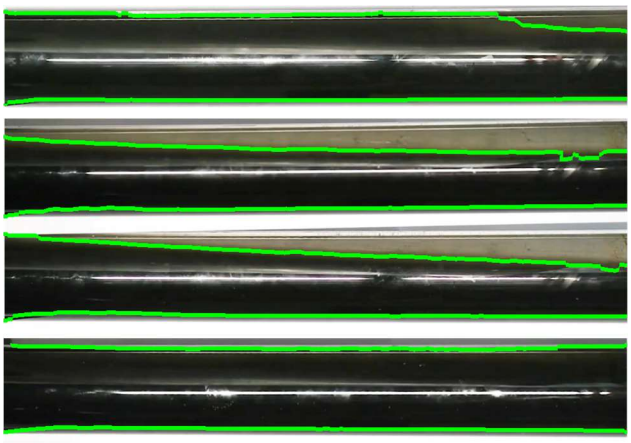

Figure B.8 – Image analysis of Figure 4.9

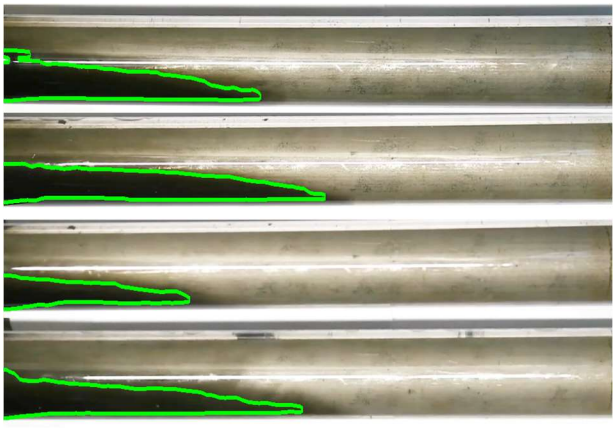

Figure B.9 – Image analysis of Figure 4.10

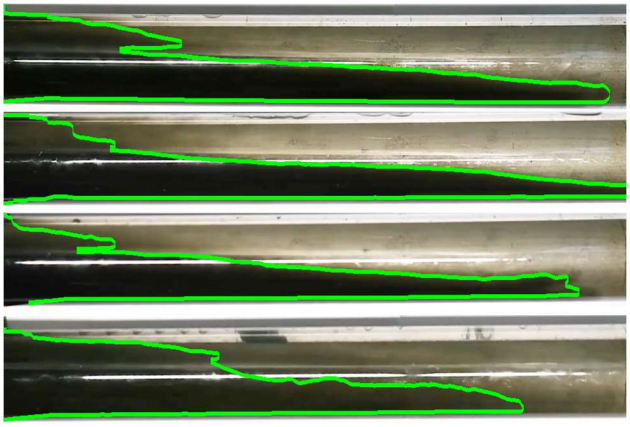

Figure B.10 – Image analysis of Figure 4.11

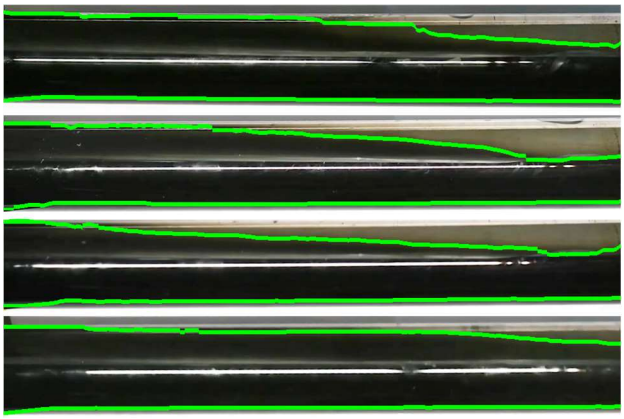

Figure B.11 – Image analysis of Figure 4.12

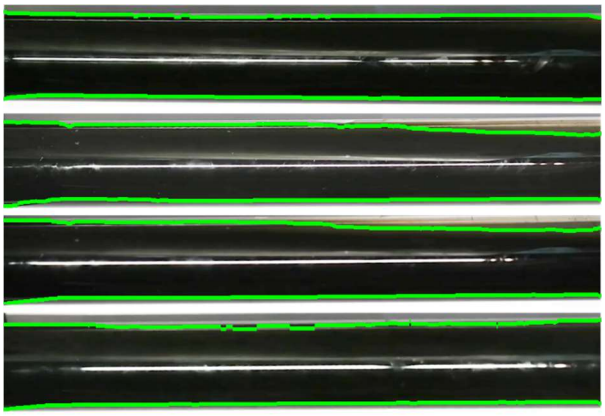

Figure B.12 – Image analysis of Figure 4.13

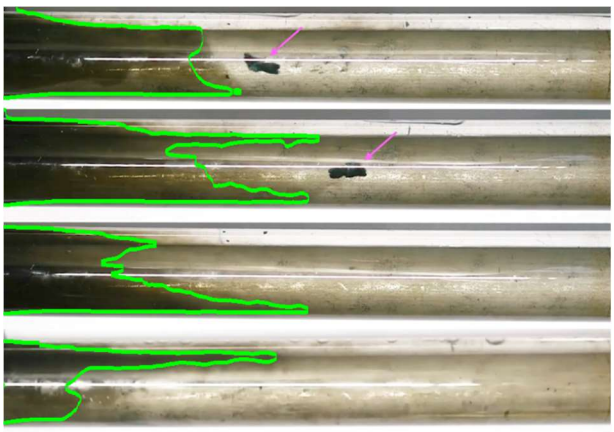

Figure B.13 – Image analysis of Figure 4.14

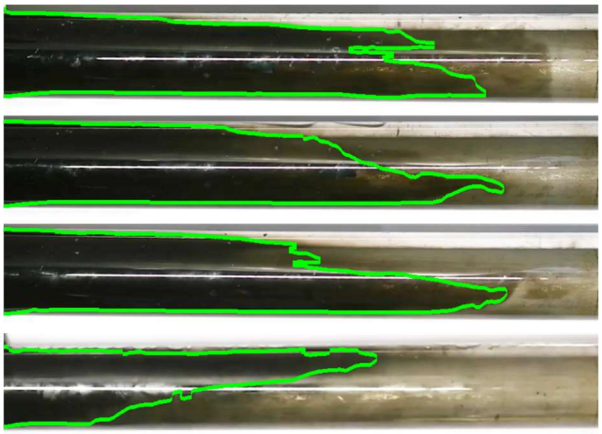

Figure B.14 – Image analysis of Figure 4.15

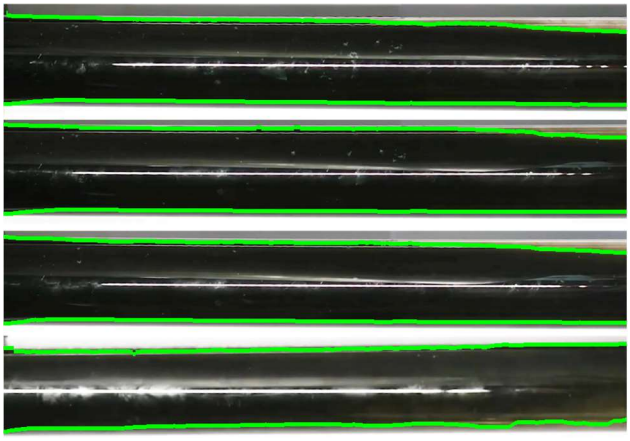

Figure B.15 – Image analysis of Figure 4.16

Appendix C – Calculation of weight material of displacing fluid

The following calculations was performed to find the correct volume of the weighing material of displacing fluid to achieve the desired density:

$$Mass_{total} = Mass_{glucose} + Mass_{water}$$

$$\rho_{total} \cdot V_{total} = \rho_{glucose} \cdot V_{glucose} + \rho_{water} \cdot V_{water}$$

$$\rho_{total} \cdot (V_{glucuse} + V_{water}) = \rho_{glucose} \cdot V_{glucose} + \rho_{water} \cdot V_{water}$$

$$\rho_{total} \cdot V_{glucuse} + \rho_{tota} \cdot V_{water} = \rho_{glucose} \cdot V_{glucose} + \rho_{water} \cdot V_{water}$$

$$\rho_{total} \cdot V_{water} - \rho_{water} \cdot V_{water} = \rho_{glucose} \cdot V_{glucose} - \rho_{total} \cdot V_{water}$$

$$V_{water} \cdot (\rho_{total} - \rho_{water}) = V_{glucose} \cdot (\rho_{glu} - \rho_{total})$$

$$V_{glucuse} = V_{water} \cdot \frac{(\rho_{total} - \rho_{water})}{(\rho_{glucose} - \rho_{total})}$$

The density of glucose is, $\rho_{glucose} = 1586$ kg/m^3

The density of total solution (desired density) is, $\rho_{total} = 111$ kg/m^3

The density of water is, $\rho_{glucose} = 998$ kg/m^3

Volume of water used = 0.016 m^3

Inserting numbers into the above calculated equation (in sg) :

$$V_{glucuse} = 0.016 \cdot \frac{(1.11 - 0.998)}{(1.586 - 1.11)} = \frac{11}{2975}$$

To find the mass of the glucose we need to make ~20 kg of solution, the following step was calculated:

$$Mass_{glucose} = \rho \cdot V$$

$$Mass_{glucose} = 1586 \cdot \frac{11}{2975} = 5.86\ kg$$

Checking if this results in ~20 liter of solution:

$$V_{total} = V_{glucose} + V_{water}$$

$$V_{total} = \frac{11}{2975} + 0.016 = 0.197\ m^3 \cdot 10^3 = 19.7\ liter$$

Hence, the calculations show that 5.86 kg of glucose is needed to make 19.7 liter of solution with the desired density of 111 kg/m^3.